CHAPTER 91

Hydrogen Effects on Plasticity

I.M. ROBERTSON, H.K. BIRNBAUM

Department of Materials Science and Engineering, University of Illinois, Urbana, IL 61801, USA

and

P. SOFRONIS

Department of Mechanical Science and Engineering, University of Illinois, Urbana, IL 61801, USA

1572-4859, DOI: 10.1016/S1572-4859(09)01504-6

Dislocations in Solids
Edited by J. P. Hirth and L. Kubin

Contents

1. Introduction

The very dramatic and deleterious effects of hydrogen on fracture have motivated many studies of the influence of hydrogen on the mechanical properties of metals. Hydrogen is a ubiquitous solute and is present in metals, in many cases inadvertently, as a result of processing, corrosion, etc. In the course of attempts to understand the mechanisms of hydrogen embrittlement [1], a wide range of observations have been made on the interaction of hydrogen with dislocations and on changes it induces in the macroscopic stress–strain response of metals. Many of these studies suffer from a number of shortcomings. Since hydrogen embrittlement presents a serious technical problem, many studies were carried out on commercial alloys, the complexity of which mitigates against the development of a mechanistic understanding of the phenomena observed. In addition, many studies were not designed to focus on the mechanism(s) by which hydrogen affects plastic behavior, in that they did not take the ''special'' properties of solute hydrogen into account. In this paper, we review observations of the effects of hydrogen on the plastic deformation of metals reported in the literature, choosing those that contribute to an understanding of the basic hydrogen–dislocation interactions as these dictate the plastic response of metals. We do not attempt to review the voluminous literature in detail [2].

Hydrogen differs from other solutes in several very important respects and these need to be kept in mind as we attempt to understand the effects of H on dislocations and plasticity. Many of these parameters enter into the understanding of the diverse behavior of different systems. What follows is a brief description of some of these parameters.

Hydrogen resides in interstitial octahedral and tetrahedral sites in bcc, fcc, and hcp metals. In bcc systems, the occupied site depends on the system and can be either the tetrahedral or the octahedral site, although for the systems for which site occupancy has been determined the tetrahedral site is favored [3]. As an example, in the V–H system the site occupied depends on the phase being considered and at high temperatures in the disordered α-phase it occupies the tetrahedral site whereas in the ordered β-phase it occupies the octahedral site [3]. In Nb and Nb-alloys, H occupies the tetrahedral site except in the $Nb_{0.5}V_{0.5}$ alloy in which it occupies both sites [4]. In fcc metals, H occupies predominantly the octahedral site (Pd [5], Ni, FCC YH_x [6], austenitic fcc Fe–Cr–Mn–Ni steels [7]), although there are reports of H occupying the tetrahedral site (FCC TiH_x, TiD_x, and YH_x [6]) – both sites have cubic symmetry. In hcp metals, H occupies the tetrahedral site [8–10].

The octahedral and tetrahedral sites posses a tetragonal symmetry and assuming a coordinate system with the tetragonal axis along the 3-direction, the strain field

can be expressed as:

$$[\varepsilon] = \begin{bmatrix} \varepsilon_{11} & 0 & 0 \\ 0 & \varepsilon_{22} & 0 \\ 0 & 0 & \varepsilon_{33} \end{bmatrix} \quad \text{with} \quad \varepsilon_{11} = \varepsilon_{22}. \tag{1}$$

Despite the tetragonal interstitial site symmetry, the distortion field associated with H in bcc systems has, based on diffuse neutron scattering [11,12] and Huang diffuse X-ray scattering [12,13], cubic symmetry. This indicates that $\varepsilon_{11} = \varepsilon_{22} = \varepsilon_{33}$. This cubic symmetry is an indication that the interstitial has strong interactions with more than first nearest-neighbor sites and that these longer-range force constants reduce the tetragonality of the distortion field [12]. Despite the fact that its atomic size is small, hydrogen has a large partial molal volume of solution, V_H, and hence a large distortion field. Curiously, V_H is a constant fraction of the atomic volume in most bcc systems and is constant, independent of composition, H/M, over the complete range of solid solutions in fcc systems [12]. For bcc systems, $V_H \sim 0.17\Omega$, where Ω is the atomic volume. For fcc systems, V_H/Ω will vary by about a factor of 3, while the actual value of V_H is approximately constant at $V_H = 2.9\,\text{Å}^3$. The importance of the distortion field around the H interstitial in determining its effect on the mechanical properties stems from the fact that the primary interaction with dislocations appears to be that of an elastic stress center. Thus, the observation that the distortion field has cubic symmetry suggests that the interaction of H with screw dislocations is not due to the deviatoric components of the distortion field but may be attributed to a second-order interaction caused by the local elastic moduli change close to the H interstitial. On the other hand, the interaction with edge dislocations would result from the dilatational components of the distortion field as well as from the local moduli changes.

Hydrogen has a very significant effect on the acoustic elastic moduli of those systems in which measurements have been made. The effects are different for H in bcc and in fcc systems. High-frequency measurements over a very wide range of H/M and temperature [14,15] have shown that in Nb, Ta, and V, H increases the bulk modulus $B = (C_{11}+2C_{12})/3$ and the shear modulus C_{44}, and decreases the shear constant, $C' = (C_{11}-C_{12})/2$. Hydrogen effects on the higher phonon frequencies show that for bcc metals, H increases all phonon branch frequencies in the three principal directions [16]. Since the transverse frequency in the $\langle 100 \rangle$, $T_{100} = C_{44}$, and the longitudinal frequency in the $\langle 110 \rangle$, $L_{110} = (C_{11}+C_{12}+2C_{44})/2$, are both increased by H, these effects are consistent with the lower frequency acoustic measurements. However, the transverse mode $T_2 = (C_{11}-C_{12})/2 = C'$ also increases with H/M in contrast with the lower frequency acoustic measurements in which C' decreases with H/M. This dispersion with frequency has not been explained, although it may be evidence for an H Snoek effect (a relaxation phenomenon associated with solute redistribution) – an effect that has not otherwise been seen. The effects of H on the elastic properties indicate that changes in the electronic structure of the solids play an important role in determining these properties. Since the lattice expansion that accompanies solution of H would

normally be expected to lead to a decrease in the phonon frequencies, the increases seen in the bcc systems are clearly due to electronic effects. Phonon dispersion measurements in the Pd–H system [16] do show the expected decrease in the frequencies associated with the lattice expansion.

Another way in which H differs from other solutes is its very high mobility [17]. While diffusion of H in metals results from phonon-assisted tunneling at temperatures below $\sim 20\,\mathrm{K}$ [18], in the temperature range important to hydrogen effects on plasticity, the temperature dependence of the diffusivity can generally be described by an Arrhenius relation. The diffusivity of H is extremely high in the vicinity of 300 K and its behavior is characterized by very small activation enthalpies (see Table 1).

In addition to the high H diffusivities, the mobility of H is very dependent on trapping at lattice defects [19]. As a consequence, the effective diffusivity, D_{eff} is described by:

$$D_{\mathrm{eff}} = D\frac{K}{K + (aN_{\mathrm{T}})/(\beta N_{\mathrm{L}})(\theta_{\mathrm{T}}/\theta_{\mathrm{L}})}. \tag{2}$$

In eq. (2), D is the lattice diffusivity; N_{T}, the density of traps; α, the number of hydrogen atoms that can be accommodated per trap; N_{L}, the density of the solvent atoms; β, the number of lattice interstitial sites per solvent atom; θ_{T} and θ_{L}, the occupancies of the trap and lattice sites, respectively; and $K = \exp(\Delta E/kT)$, the equilibrium constant with ΔE being the trapping enthalpy, k, Boltzmann's constant, and T, the absolute temperature. Equilibrium between H in traps and lattice sites is given by:

$$\frac{\theta_{\mathrm{T}}}{1-\theta_{\mathrm{T}}} = \frac{\theta_{\mathrm{L}}}{1-\theta_{\mathrm{L}}}\exp\left(\frac{\Delta E}{kT}\right). \tag{3}$$

Experimentally it is observed that H is trapped in a large variety of defects and some examples are given in Table 2 [20–30]. Most traps are "saturable," i.e., they achieve an equilibrium H concentration, and the remainder of the H is in interstitial

Table 1
Hydrogen diffusivity in metals (see Ref. [17])

System	Diffusivity at 300 K ($\mathrm{m^2\,s^{-1}}$)	Activation enthalpy (eV)
Pd (fcc)	3.9×10^{-11}	0.230
Ni (fcc)	6.0×10^{-14}	0.420
Fe (bcc)	1.6×10^{-8}	0.069
Steels (bcc)[a]	1.5×10^{-9}	0.083
Stainless steels (fcc)[a]	1.7×10^{-16}	0.561
Nb (bcc)	8.2×10^{-10}	0.106
Ta (bcc)	1.9×10^{-10}	0.140
V (bcc)	5.4×10^{-9}	0.045

[a]H diffusivities in these systems depend on the particular compositions.

Table 2
Examples of hydrogen traps

System	Trap	Trapping enthalpy (eV)	Ref.
"pure Fe"	Dislocations	0.62	[20]
"pure Fe"	Vacancies	0.63	[22]
"pure Fe"	Ti solutes	0.19	[22]
"pure Fe"	C interstitials	0.03	[22]
"pure Fe"	N interstitials	0.13	[22]
Ferritic steels	Ti–C precipitates	1.0	[22]
Ferritic steel	Fe_3C boundaries	0.11	[22]
fcc stainless steel	γ' boundaries	0.10–0.15	[22]
Niobium	N interstitials	0.12	[22]
Niobium	O interstitials	0.09	[26]
Niobium	H–H pairs	0.06	[26]
Nickel	Substitutional solutes	0.08–0.12	[25]
Nickel	Vacancies	0.44	[22]
Nickel	Grain boundaries	0.12	[24,31]
Aluminum	Vacancies	0.52	[22]
Aluminum	Grain boundaries	0.15	[22]
Palladium	Vacancies	0.23	[22]
Palladium	Dislocations	0.6	[22]

lattice sites. The experimental values of the binding enthalpies indicate very strong trapping at defects in the temperature range of interest for plasticity and dislocation studies.

In systems such as ferritic steels and stainless steels, the H diffusivity is greatly reduced by the presence of traps [17,19] making it difficult to categorize the effects of H on plasticity without taking this into account. In the vicinity of 300 K, the range of D_{eff} in different steels is about four orders of magnitude lower than in pure metals as a result of trapping effects.

As discussed in greater detail in the body of this paper, the mobility of H affects dislocations and plasticity in several ways. These include:

a. the kinetics of formation of H atmospheres around dislocations and other elastic stress centers,
b. the response of these atmospheres to changes in the local chemical potentials and stresses,
c. the amount of H available for the formation of these atmospheres,
d. the stress gradients and damage created when H is introduced into the lattice, and
e. the formation of second phases such as hydrides before and during deformation.

A good deal of the controversy over the effects of H on plasticity and the stress–strain response of solids has arisen due to neglect of the kinetic factors associated with the interaction of H with dislocations. In the temperature range where these

studies have been carried out, the kinetic aspects of the interactions must be considered. This is in contrast to most other solutes that in the temperature range of interest are much less mobile than H and hence can be treated as fixed pinning points.

Since H is an ''incidental'' or ''accidental'' solute addition to most metals, the interest in its effect on dislocations and plasticity stems from its connection with ''hydrogen embrittlement.'' In many systems, hydrogen embrittlement is a misnomer and the failure is the result of plastic failure processes, albeit on a very local scale [1]. This was first suggested by Beachem [32] to account for the presence of ductile features on fracture surfaces of hydrogen embrittled steels. This was a significant and noteworthy departure from all prior explanations of the presence of these features on fracture surfaces [33,34] as it suggested that plastic processes were impacted directly by hydrogen and were not simply a consequence of the hydrogen-enhanced fracture event. Since that early suggestion, a large number of observations have supported the conclusion that in many systems, hydrogen embrittlement results from locally ductile failure. *In situ* environmental cell TEM deformation and fracture studies have shown that the basic processes of hydrogen-related fracture are local plastic failure in regions in front of the crack tip [35–46]. These enhanced plastic processes are not restricted to the locale of the crack tip but occur at distances up to 1×10^{-6} m ahead of it. A critical feature is that the enhanced plasticity processes are confined to a specific and narrow region [47,48] that ultimately is manifested in the appearance of the fracture surfaces. A unique aspect of this type of fracture is that the presence of hydrogen in the environment, or in solid solution, results in the dynamic maintenance of a high concentration of solute hydrogen close to the crack tip. As clearly shown in the *in situ* TEM deformation studies, hydrogen causes local plastic deformation at stresses below that required in the absence of H or when H is uniformly distributed in solid solution. Dislocation velocities near the crack tips are greatly increased when the environmental cell atmosphere is changed from vacuum or inert gas to hydrogen gas. Similar results were obtained using water vapor in the case of Al and Al alloys [38,39]. These results, discussed in greater detail below, caused the crack to proceed by ductile failure process at or immediately in front of the crack tip. Since the plasticity proceeds at significantly lower stresses than that required to cause deformation of the volume away from the crack tip (where the H concentration was lower), the failure occurs in the absence of macroscopic deformation – hence giving the impression of ''embrittlement.'' These observations formed the basis for the HELP (hydrogen enhanced localized plasticity) mechanism of hydrogen embrittlement [1].

Of course, the HELP mechanism for hydrogen embrittlement, while observed for bcc [35,36], fcc [37,39,49], and hcp [40] pure metals, and alloys [38,42–44,46,50] is not the only hydrogen embrittlement mechanism. Clear evidence, by direct observation as well as *a posteriori* studies, indicates that other mechanisms of hydrogen embrittlement also are operative, with the actual mechanism depending on the circumstance. In systems where hydrides can be formed, e.g., Nb, V, Ta, Zr, Mg and Ti, stress-induced hydride formation and cracking is generally the dominant environmental fracture mechanism [51]. Even in these studies, hydrogen-enhanced

dislocation motion is observed but the failure occurs because the hydride fails by cleavage. For example, in hcp α-Ti [40] failure occurs at a low stress intensity and slow crack growth rates by the formation and fracture of a stress-induced hydride. However, at higher imposed stress intensities and faster crack growth rates, failure is by the HELP mechanism since the crack is driven faster than the formation and growth rate of hydrides ahead of the crack. In systems in which both mechanisms are viable, the one that dominates is determined by the kinetics of hydride formation or H solute segregation to dislocations at the crack tip. Both are competitive with the alternative of general ductile fracture that will occur if failure due to either H-related mechanism does not precede it.

As the HELP and the stress-induced hydride formation and cleavage mechanisms depend on H mobility, they offer an intrinsic explanation for why the embrittlement disappears at low and at high temperatures. At low temperatures, the mobility of H is reduced and general ductile failure occurs before the HELP or the hydride mechanism can intervene. At low temperatures in hydride-forming systems, hydride precipitation occurs in the absence of external stress stabilization and the hydrides act as any other brittle phase cracking under stress, but the propagation of the fracture between hydrides is by normal ductile failure mechanisms. At high temperatures in hydride-forming systems, stress stabilization of the hydrides is not sufficient and the material behaves in a ductile manner. As was discussed in some detail [1], the HELP mechanism also does not lead to failure at temperatures at which the H is uniformly distributed in the lattice rather than in dislocation atmospheres.

Although hydrogen-enhanced fracture is not the emphasis of this paper it should be noted that an alternate explanation is associated with hydrogen reducing the effective lattice cohesive strength – the so-called decohesion model [52]. This reduction is a consequence of interstitial hydrogen changing the local and global atomistic [53] and electronic structure [54,55], as well as increasing the separation distance between atoms. Liang and Sofronis [56,57] studied intergranular failure of Ni-based alloys by considering the effect of hydrogen on fracture in terms of how it influences the cohesive properties of the grain boundary and the grain boundary carbide/matrix interfaces, the failure of which is resisted by cohesive tractions. The determination of the effect of hydrogen on the cohesive tractions [58] was carried out on the basis of the fast separation limit of the Hirth and Rice thermodynamic theory of interfacial decohesion [59]. Such a cohesive element approach was also undertaken by Serebrinsky et al. [60] to study hydrogen-assisted crack propagation in bcc iron systems. The fundamental idea in this model is that hydrogen reduces the ideal work of fracture along {1 1 0} planes as determined by density functional theory [61,62]. On the basis of these *ab initio* calculations, the authors predict that a sufficient amount of hydrogen is available to fracture transgranularly a system such as bcc iron. The difficulty with these cohesive element approaches is achieving and more importantly maintaining the critical hydrogen concentration ahead of a propagating crack. More recently, through modeling intergranular crack propagation in IN903 superalloy, Dadfarnia et al. [63] pointed to several shortcomings of the decohesion theory in predicting the experimentally measured fracture response.

These investigators used a traction-separation law derived from the thermodynamic theory of interfacial decohesion of Mishin et al. [64]. Unlike the Hirth and Rice theory, the Mishin et al. approach addresses quantitatively interfacial separation at stages between the fast and slow separation limits.

2. Experimental observations

2.1. Macroscopic measurements of plastic flow properties

Early studies of the effects of solute H on the deformation of solids often gave conflicting results. A review of the literature suggests that this confusion resulted primarily from two aspects of the experiments; namely, the method of introducing hydrogen and its effect on the defect population, and the strain rate of the test. Hydrogen often was introduced from high-fugacity sources, either from the gas phase or from electrolytic solutions by cathodic charging, and at temperatures where the H diffusivity was somewhat limited. A consequence of high-fugacity charging is ''near surface damage,'' such as the formation of voids and pressurized H_2 gas bubbles. When these defects form a decrease in the flow stress, termed softening, is often observed [65,66]. Another consequence of high-fugacity charging is that the large lattice expansion that accompanies the high surface concentrations generates a stress gradient [67,68] and, in addition to the effects of residual stresses, causes high dislocation densities in the near surface region that lead to surface hardening [69]. In unstable stainless steels, this ''near surface damage'' can include stress-induced martensitic phases [67,70,71] and these act as barriers to dislocation egress through the surface. The high dislocation densities and the residual stresses generally lead to an increase in the flow stress. Thus it is immediately evident that different effects can result from high-fugacity charging and this is system dependent.

Hydride-forming systems have been less well studied with respect to the effects of H on their deformation behavior. In these systems attention has focused on the stress-induced hydride formation and cleavage mechanisms which leads to brittle behavior in a limited temperature range [51]. Hydrides formed during charging can have several roles in influencing the deformation processes. Cathodic charging of systems such as Ni [72], Pd, Ti, etc. can cause the formation of a very hard, brittle hydride at the surface. In the case of Ni, this ''hydride'' (actually the β-phase solid solution) forms a continuous coating on the surface with the attendant formation of a high compressive stress and a barrier to the egress of dislocations [73]. Deformation during charging results in the cracking of this hydride and the decrease in the cross section of the specimen, followed by further ''hydride'' formation. The process causes an increase in the apparent flow stress of the specimen and a decrease in the strain to failure. In other systems, the formation of the hydride plays a dual role. Small hydride particles can act as barriers to dislocation motion leading to hardening. However, due to the very large volume of formation of hydrides, their formation and growth is accompanied by the

generation of high densities of accommodation dislocations [40,74] and these can serve as dislocation sources leading to softening. Again in these systems, H charging can lead to a duality of behaviors.

A clear demonstration of the importance of avoiding damage during the introduction of H was provided by Kimura and Birnbaum [73] who studied the effects of cathodic charging during deformation at rates between 2×10^{-6} and $8 \times 10^{-5}\,s^{-1}$ in Ni and Ni–C alloys. At high cathodic current densities, decreases in the flow stress were observed during charging and increases once charging ceased. At low current densities, small transient increases in flow stress were observed. The effects were largest in the temperature range where significant H diffusion into the specimen can be expected. In all cases, cathodic precharging caused insignificant increases in flow stress and was shown to be the result of formation of surface hydrides. These results are consistent with the creation of lattice damage in the surface region; e.g., the introduction of dislocations in the near surface region during the dynamic charging experiments. Such an increase in the mobile dislocation density would appear at the macroscale as softening. Precharging as well as simultaneous charging during the test can produce a thin surface "hydride" (the β-phase) which hardens the surface and thus prevents the egress of dislocations. This results in an increase in flow stress once the charging is stopped and no further dislocation injection occurs.

The second factor that can lead to seemingly disparate results is the strain rate at which the mechanical property tests are conducted. Strain rate effects are coupled to temperature effects and will be discussed in detail later. However, at this point it should be noted that interstitial H can act as a solute pinning point and impede the motion of dislocations leading to hardening when tests are performed at strain rates and temperatures under which H is immobile. At low strain rates, when H can move in response to the changing stress field of a passing dislocation, solute H can lead to decreases in the flow stress, i.e., softening. This fact was not recognized in the early studies as they were often carried out at relatively high strain rates. Interestingly, the strain rate and temperature effects observed for the plastic response in the presence of H are closely related to those observed for H effects on fracture.

In the following discussion, we focus attention on the effects of H on plastic deformation in those cases where the H charging does not cause structural damage e.g., void formation and H bubble formation. In the early observations of the stress–strain response of ferritic and stainless steels, when H was added to the material the yield and flow stresses increased, as did the work hardening rate [75]. These experiments were carried out on precharged specimens at temperatures between 300 and 200 K and at strain rates of the order of $10^{-4}\,s^{-1}$ using a wide range of grain sizes. Similar increases in the yield and flow stress were reported for 99.8% Ni polycrystals and single crystals, that were either cathodically precharged or charged during the tensile tests, were obtained at strain rates of about $10^{-4}\,s^{-1}$ [76–80]. These tests also showed serrated yielding at room temperature and at lower temperatures, consistent with dislocation pinning by H.

In the absence of the formation of voids, gas bubbles, or fissures, severe charging with H has generally been observed to lead to hardening, i.e., an increase in the

flow stress for both single crystals and polycrystalline specimens of Fe [65,81,82], ferritic, and stainless steels. Increases in the flow stress can result from the introduction of a high near surface dislocation density and surface compressive stress due to the H concentration gradient developed during charging, or due to the formation of more effective point defect pinning points from C–H or N–H clusters. Measurements of the flow stress in H-charged Fe as a function of grain size have been interpreted using the Hall–Petch relation:

$$\sigma_f = \sigma_0 + K_f d^{-1/2} \tag{4}$$

In eq. (4) σ_f is the flow stress; σ_0, the lattice frictional stress; K_f, the Hall–Petch slope that measures the strength of the grain boundaries to slip propagation; and d, the grain size. In H precharged Fe, Adair [83] observed low yield points and found that the Hall–Petch analysis indicated an increased friction stress and a decreased Hall–Petch slope, whereas in tests conducted with simultaneous H charging, Bernstein [84] observed the opposite effect – a decreased σ_0 and increased K_f. While these disparate observations may reflect differences in material purity or charging conditions, it is difficult to make a definitive decision on the basis of what is known. However, the results are consistent with the injection of dislocations in the case of deformation and simultaneous charging [84] and the possible formation of small gas bubbles in the precharged specimens [83] where the cathodic charging conditions were considerably more severe.

Experiments by Lunarska and Wokulski [85] on Fe whiskers are of interest as these single crystals contained a relatively low as-grown dislocation density. Tensile tests at strain rates between 2 and $11 \times 10^{-4}\,s^{-1}$, high rates for hydrogen effects, were carried out with simultaneous cathodic charging under high H-fugacity conditions. Once plastic deformation began these whiskers exhibited significant decreases in flow stress when H charging was started and rapid recovery of the flow stress when H charging ceased. These observations can be interpreted as due to the injection of dislocations during the charging periods. Slip lines in the absence of H charging were ''wavy'' and localized to the region near the failure ''neck'' whereas those in the H-charged specimens were planar and more uniformly distributed along the length of the specimen, again consistent with the injection of dislocations during the H charging.

High-fugacity H charging causes structural damage and has a major effect on the deformation properties of high-purity Al (99.999% purity) [86]. Introduction of large amounts of H in Al can be achieved either by cathodic charging or by etching in NaOH aqueous solutions. This resulted in very large softening of the tensile flow stress and severe slip localization (Figs 1 and 2). While this was originally interpreted as due to solute H, neutron scattering, TEM and SEM studies [87] have shown that the hydrogen is present as gas bubbles ranging in size from about 2 nm to 35×10^{-6} m (Fig. 3). Apparently, the presence of a large number of gas bubbles resulted in the softening behavior as well as shear localization.

To demonstrate that the macroscopic property changes depended on the conditions under which hydrogen was introduced, a low-energy H^+ ion plasma

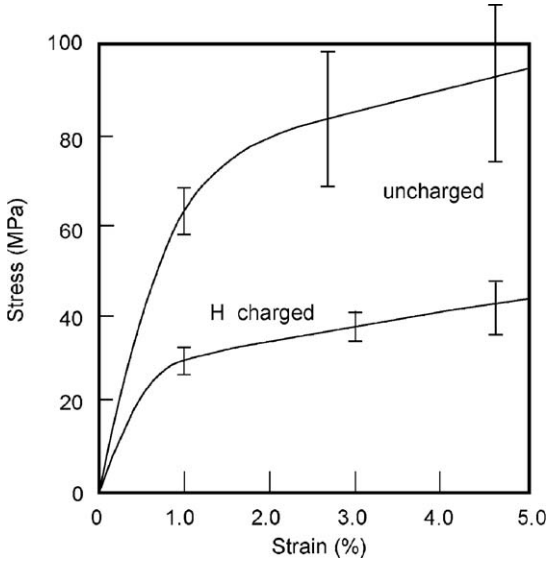

Fig. 1. Stress–strain curves for high purity Al (99.999% purity) polycrystalline specimens in the uncharged state and with Al/H $\sim 2 \times 10^{-3}$ H added by cathodic charging. Each curve is the average of 25 tests with the error bars determined from the repeated measurements. Reprinted from Ref. [86] with permission from Elsevier.

was employed to introduce hydrogen to thin specimens of pure iron (99.99% purity) [88]. Due to the high-energy reference state of the H^+ ions a high-fugacity condition is obtained and significant H/M values can be achieved without the concomitant near surface damage. When this charging method was used during tensile deformation, significant decreases in the flow stress of Fe were observed over the temperature range from 77 to 300 K [88]. A maximum decrease in the flow stress was observed in the vicinity of 200 K. This softening is believed to be due to dislocation–hydrogen interactions and to neither surface damage nor dislocation injection, as judged by comparing the effects in the H plasma with those observed in inert gas plasmas.

As can be seen from the above discussion, the situation in metals of relatively high purity and in steels is complex because of competing factors. In another system of interest, stainless steels, the possibility of H and stress-induced phase transitions must be considered too [67,71,89]. Altstetter et al. have measured the tensile properties of stable 310 and unstable 304 stainless steels at strain rates in the range from 10^{-3} to $10^{-6}\,s^{-1}$ and at temperatures between 77 and 295 K [90,91]. The yield and flow stresses of both alloys were increased by the addition of solute H. In both steels, high H concentrations caused the formation of a γ*-"hydride" [67,71,92] and in the unstable steels H stabilized the formation of α' and ε martensite. These induced phases provide barriers to dislocation motion. In the 310 SS, increases in the flow stress were observed at H/M values well below that required for the formation of the γ*-phase. Altstetter et al. proposed that in view of the fact that the γ*-phase has a large volume of formation it can be stress stabilized in dislocation

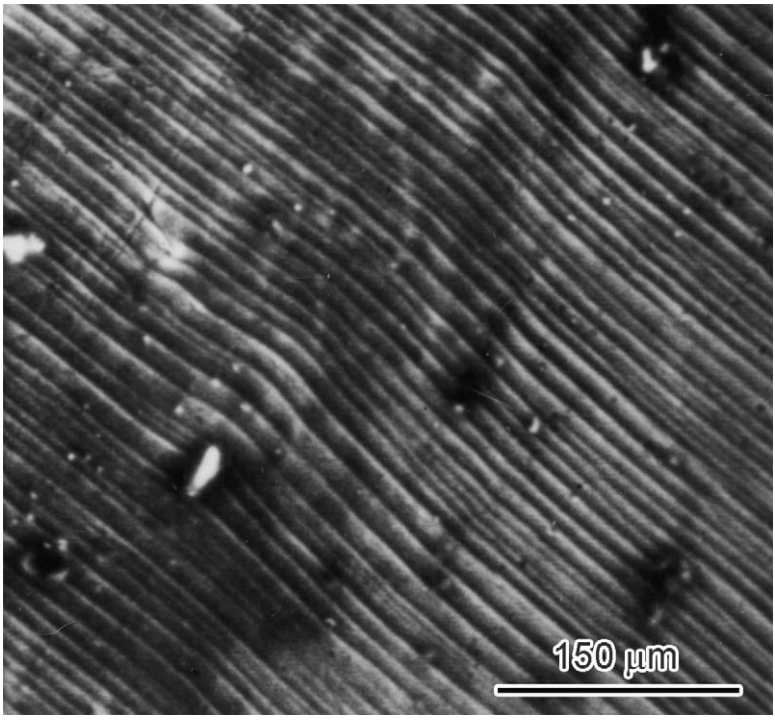

Fig. 2. Micrograph showing coarse slip lines due to shear localization in high purity Al (99.999%) cathodically charged with H ($H/M = 2 \times 10^{-3}$). Reprinted from Ref. [86] with permission from Elsevier.

cores at low H/M [93–95]. Thus, the increase in the flow stresses observed for stainless steels on adding solute H could be caused by stress-enhanced phase transitions at relatively low H/M. However, severe strain localization is observed in both stainless steels [90,91] and this can also result in an increase of the tensile flow stress.

Another approach to examining the effect of H on plasticity was pursued using cathodic charging at current densities of $1.0\,A\,m^{-2}$ during creep measurements [96]. These experiments revealed an initial decrease in the transient creep strain and strain rate as the H/M value increased. At longer times, the transient creep rates in the presence of H remain high and hence the creep strain at long times with H is greater than in uncharged specimens. Consistent with these measurements, low-pressure hydrogen atmospheres were observed to markedly decrease the creep rupture lifetime of Fe–Ni alloys at elevated temperatures [97]. This effect was not due to the formation of gas bubbles of H_2 or CH_4 or any other structural changes. The steady-state creep rate was not affected by H, nor was the extent of grain boundary sliding. The extent of steady-state creep (Stage II) was markedly shortened in the presence of the H and the specimens failed by entering tertiary creep (Stage III) at a significantly lower total creep strain. In contrast to these

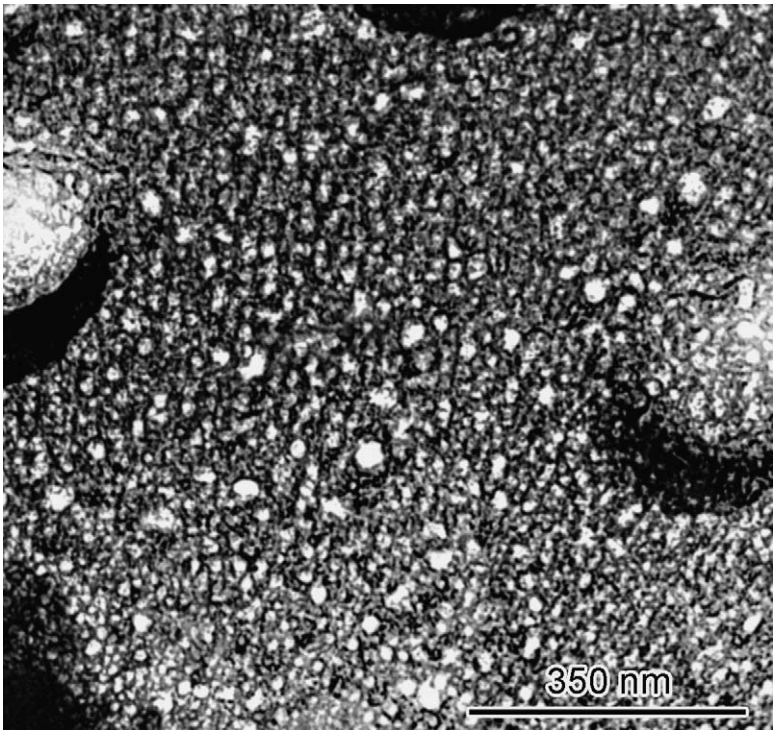

Fig. 3. TEM image of high purity Al (99.999%) charged with H to H/M $= 2 \times 10^{-3}$. The charged Al showed a range of H_2 bubbles with sizes between about 2 to 35 mm (Image courtesy of R. Pickerill and I. M. Robertson).

measurements in non-hydride forming systems, the addition of H to α-Ti alloys [98] resulted in a large increase in the transient creep strain once a critical H/M was exceeded. This increase was attributed to the formation of hydrides and to the dislocations that accommodate the volume changes associated with hydride formation acting as generators of dislocations [40,74].

Perhaps the strongest evidence for decreases in the tensile flow stress due to H charging is provided by the series of papers by Kimura et al. [99–103] on Fe of various purities. Zone-refined Fe having a residual resistivity ratio, RRR $= (\rho_{273}/\rho_{4.2})$, of about $\sim$5500 did not show any evidence for hydrogen damage (surface blistering) after cathodic charging at 20 A m^{-2} at temperatures around 295 K, while less-pure specimens did show permanent surface damage. In slow strain rate tests, $\dot{\varepsilon} = 8 \times 10^{-5}$ s^{-1}, with concurrent cathodic charging an immediate decrease in the flow stress was observed. On ceasing the charging there was an almost immediate increase in the flow stress which continued with a high work hardening rate. This decrease on charging and increase on cessation of charging could be repeated during the course of the tensile test. The decrease in the flow stress was greatest at about 200 K and decreased as the strain rate increased. These

effects were less pronounced in lower purity specimens (RRR = 1800) where small increases in flow stress preceded the decreases.

Cathodic precharging of H into the high-purity Fe with a current density of 100–300 A m^{-2} (considerably higher than was used in the experiments where the H charging occurred during the straining) resulted in decreases in the flow stress [100]. The largest effects were observed in the highest purity specimens and with the shortest aging time after charging. As with the experiments in which charging occurred during deformation, the decreases in flow stress were greatest at test temperatures of about 200 K. The response of high-purity Fe (RRR ~ 5000) single crystals to hydrogen were studied with similar techniques and they showed decreases in the flow stress, particularly in the early parts of the stress–strain curves and at temperatures of about 200 K.

However, in the experiments by Kimura et al. [99–103], at temperatures below 190 K the decrease in flow stress on beginning cathodic charging was temporary and then it increased as deformation and charging continued. No structural characterization to determine the extent and nature of the damage due to the charging was reported. To discover the induced-damage state, Tabata and Birnbaum conducted a TEM investigation on similarly charged material. They found that whereas cathodic charging at the low-current densities did not cause any near surface damage at room temperature, at a charging temperature of about 200 K, small H_2 bubbles were formed in the near surface region. An example of these bubbles is shown in the image presented in Fig. 4. If these bubbles were present in the samples used in the studies by Kimura et al. [99–103] they would serve as obstacles to dislocation motion and thus would provide an explanation for the observed increase in flow stress on charging below 190 K.

Oguri et al. [102] studied Fe–C alloys prepared from high-purity zone-refined Fe. Under cathodic charging conditions, using current densities of 10 A m^{-2}, they observed both softening and hardening in the temperature range 170–295 K at a strain rate of 8×10^{-5} s^{-1}. In these alloys, small amounts of C gave solid solution softening [104] while at higher C concentrations, solid solution hardening was observed. In the softening range of C concentrations, the addition of H by cathodic charging during straining resulted in decreases of the flow stress with a maximum effect at about 200 K and hardening at about 273 K. At higher C concentrations, the addition of H generally caused increases in the flow stress, with the exception of a small decrease at about 200 K.

While the results of Kimura et al. [99–103] seem to clearly support decreases of the flow stress when H is added to high-purity Fe at temperatures above about 190 K, there are a number of independent factors that enter into the totality of interpretation needed to explain their results. One cannot obtain a definitive mechanistic explanation based on the information presented by their experiments. In the case of hydrogen, Kimura et al. [99–103] proposed that the observed softening was due to modification of the Peierls potential and its effect on screw dislocation mobility and the hardening at low temperatures to hydrogen at the dislocation core pinning kinks on screw dislocations. It was argued that hydrogen impacted screw dislocations only. Atomistic simulations of hydrogen effects on

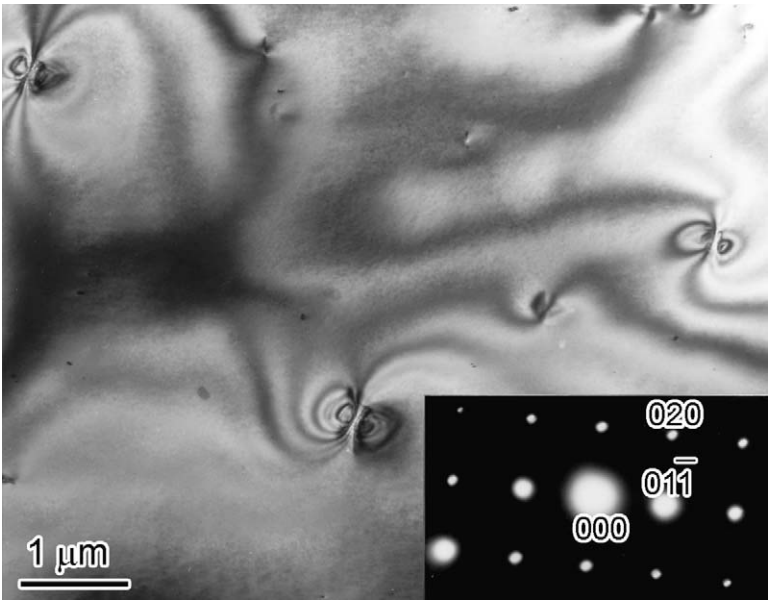

Fig. 4. TEM image of the near surface region of zone-refined Fe cathodically charged with H at 20 A m^{-2} at 200 K following the procedure used by Kimura et al. [78–82]. The defects shown are small H_2 gas bubbles as shown by dark field imaging experiments. These defects were not seen in specimens charged in the vicinity of 295 K (T. Tabata and H. K. Birnbaum, unpublished results).

kink-pair nucleation and mobility suggest that enhanced nucleation occurs when H transitions from a weaker to a stronger binding site and hardening when hydrogen–kink pair interactions occur [105]. However, the observations reported in Fig. 4 suggest that a simpler mechanism based on introduction of dislocation obstacles in the form of small bubbles may account for the low-temperature hardening. Thus, it appears that decreases in the flow stress by the addition of H may occur over the entire temperature range studied, if the superimposed hardening due to the H_2 bubbles is taken into account. In the Fe–C alloys, the hardening and softening were attributed by Kimura et al. [102] to the effects of the C and H on kink nucleation and motion on screw dislocations. In the case of C, the solid solution softening was attributed to elastic stresses imposed by the C atom on the screw dislocation which influenced kink-pair nucleation. The explanation proposed by Kimura et al. [99–103], requires what these authors considered to be a questionable set of arguments and are unable to explain all the observed results. However, at this time the importance or impact of H effects on kink nucleation and motion in bcc systems can be neither supported nor discarded definitively.

The influence of H on the properties of polycrystalline Ni having various levels of purity and C interstitial concentrations has been studied. Here H was introduced by rapid cooling from elevated temperatures in an H_2 gas atmosphere or by exposure to H_2 gas during deformation [47]. Both charging methods produced no irreversible

damage and the high-temperature charging method introduced large amounts of H (H/M = (3–7) × 10^{-4}). Significant softening was observed in the early stages of plastic deformation when specimens were tested at 300 K and at very low strain rates ($\dot{\varepsilon} = 10^{-7}\ s^{-1}$) in low-pressure H_2 atmospheres or when solute hydrogen introduced by high-temperature charging was present (Fig. 5). The decreases in the flow stress at low strains were greatest when C interstitials acted as barriers to dislocation motion. At higher strain rates (Fig. 6) there was no significant decrease in flow stress due to H, and at still higher strain rates, increases in the flow stress due to H were observed. These results clearly show the dependence of the material response to strain rate, with the level of hydrogen-induced softening decreasing with increasing strain rate.

During the many studies of the effects of H on plasticity, there have been a number of reports of serrated yielding [76,78,79,106–108]. Serrated yielding is generally attributed to the repeated pinning and breakaway of mobile dislocations from solute atoms [109]. The critical strain rate, $\dot{\varepsilon}_c$, below which serrated yielding occurs is given by:

$$\dot{\varepsilon}_c = \rho_m b v_c = 4 b \rho_m \frac{DkT}{r_c \Delta E}. \tag{5}$$

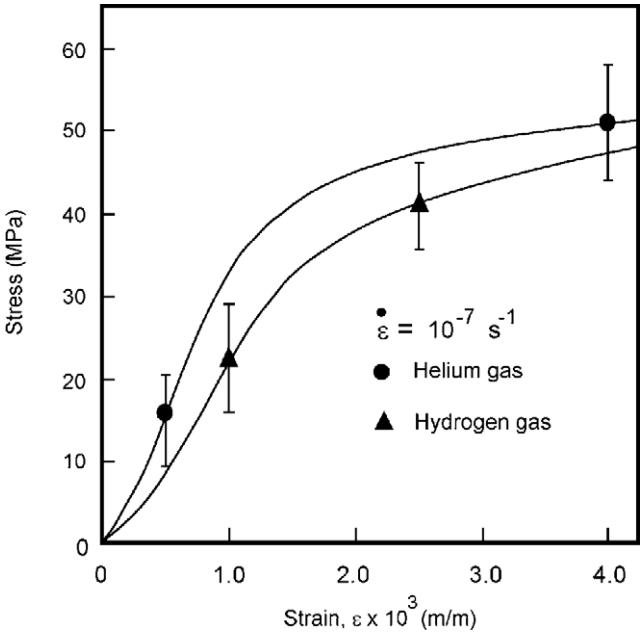

Fig. 5. Stress–strain curves for Ni containing 1200 appm C strained in H_2 (▲) or He (●) gas at 100 kPa pressure at 300 K and at a strain rate of $10^{-7}\ s^{-1}$. The specimens were 25 mm in thickness. Each curve is the average of at least seven repeated tests and the error bars indicate the standard deviations at the indicated strains. These results show a significant decrease in the flow stress when the tests were conducted in gaseous H_2. Data points omitted for clarity. Reprinted from Ref. [47] with permission from Elsevier.

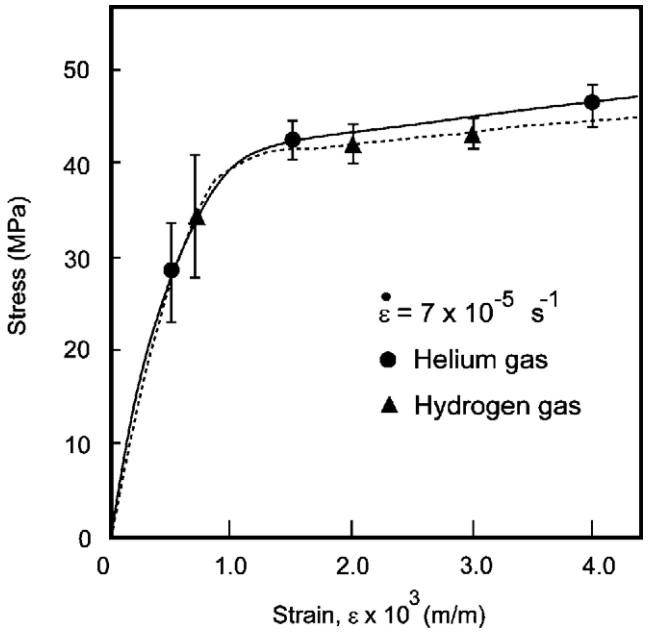

Fig. 6. Stress–strain curves for Ni containing 1200 appm C strained in H_2 (▲) or He (●) gas at 100 kPa pressure at 300 K and at a strain rate of $7 \times 10^{-5}\,s^{-1}$. The specimens were 25 mm in thickness. Each curve is the average of at least seven repeated tests and the error bars indicate the standard deviations at the indicated strains. No significant decreases in the flow stress due to H were seen. Data points omitted for clarity. Reprinted from Ref. [47] with permission from Elsevier.

Here ρ_m is the mobile dislocation density; b, the magnitude of the Burgers vector of the dislocation; v_c, the velocity at which the dislocation breaks away from the H atmosphere; D, the diffusivity; r_c, the effective radius of the atmosphere; and ΔE, the strength of the dislocation–solute interaction. For each strain rate, serrated yielding occurs within a specific temperature range with a lower bound being the temperature below which a hydrogen atmosphere cannot reform on the dislocation during the deformation process and the upper bound by the temperature at which the atmosphere keeps pace with the mobile dislocation to which it is attached i.e. $T_{lc}(\dot{\varepsilon}) < T < T_{uc}(\dot{\varepsilon})$. In Ni [108], T_{uc} was independent of $\dot{\varepsilon}$ ($T_{uc} = 227$ K) and was consistent with the temperature below which hydrides would form in the stress field of the dislocation core [93–95]. The lower critical temperature, T_{lc}, exhibited an Arrhenius temperature dependence with $\dot{\varepsilon}$, as expected from eq. (5), with an activation enthalpy of 0.57 eV at the lower strain rates and 0.25 eV at the higher strain rates. The interpretation of these values is that T_{lc} is determined by diffusion in the core of the dislocations at the high strain rates where hydrides cannot form and in the hydrides at the core of the dislocations at the low strain rates where the dislocations are moving slow enough to allow them to form.

2.2. Summary of observations

In view of the complexity of the observations relating to the effects of H on macroscopic plastic deformation, we summarize the general conclusions that can be drawn from the experiments.

- Introduction of H from high-fugacity environments causes irreversible damage in the near surface region in the form of voids, gas bubbles, high compressive stresses, high dislocation densities and in some systems ''hydrides'' or second phases. These effects are particularly significant in systems and at temperatures where the H diffusivity is low.
- Voids and H_2 gas bubbles decrease the measured tensile flow stress for deformation by decreasing the cross section of the specimen. They can also result in severe slip localization.
- Small bubbles can cause hardening by providing dislocation pinning points. Second phases, if formed, provide impediments to the egress of dislocations and thus cause hardening.
- Enhanced near surface dislocation densities can act to increase the flow stress when the specimens are precharged, due to the formation of a ''work-hardened'' surface layer. When H charging is carried out during the deformation, the dynamic injection of dislocations can lead to softening. Similarly, the dynamic formation of small hydrides during the deformation can inject dislocations into the specimen, also leading to softening whereas the static surface hydride layer formed during precharging can cause hardening.
- Intrinsic effects of H on the plastic properties of metals have been established in high-purity metals using H-charging methods that do not cause permanent structural damage. In very high purity Fe, H causes a decrease of the flow stress at temperatures above about 190 K and an increase below; the latter effect may be a consequence of small gas bubbles formed during the initial cathodic charging. In Ni, softening caused by H is seen at very low strain rates.
- Serrated yielding in Ni–H alloys below 227 K demonstrates the hardening effects of H at low temperatures and is interpreted as being caused by the repeated breakaway of dislocations from the H atmospheres (or dislocation core hydrides) and the reforming of these atmospheres.

2.3. Dislocation densities and distributions

Since solute H has been shown to affect the flow stress of metallic systems, one expects differences in dislocation structures and densities. Several studies have attempted to discern this difference and we review those that deal with the effects of solute H. Dislocation structures associated with the accommodation of the volume expansion related to hydride formation and decomposition have been reported [40,74]. These dislocation structures are distinct and, as they do not pertain to the current discussion, they are not considered further. Matsui et al. [100]

reported a higher dislocation density, as determined by a TEM study, in Fe cathodically charged at 200 K; this was the condition that yielded the greatest degree of softening. The density increases were small, changing from 3×10^8 to $6 \times 10^9\,cm^{-2}$ in uncharged material to between 3×10^9 and $6 \times 10^9\,cm^{-2}$ in the charged material. Although Matsui et al. concluded this difference was significant, the normal variability in dislocation density within and between TEM samples questions the validity of this conclusion. In Ni–H alloys, several TEM studies have reported no statistically significant difference in the dislocation densities for H-softened or hardened specimens [110,111]. Resistivity measurements [112] have indicated that there is a small increase in the generation of dislocations in Fe deformed in H_2 gas compared to those deformed in inert atmospheres.

Although the dislocation densities do not appear to be greatly changed by the presence of H in deformed specimens, there are very significant differences in the dislocation distributions caused by the presence of H. After deformation, the dislocations exhibit a high degree of slip localization and tangled dislocation structures and in the case of the steels, slip localization was associated with carbide particles [113,114]. Additional evidence for H-induced shear localization is obtained from slip-line studies in ferritic steels [115–118], in the ferrite phase of duplex stainless steels [119], and in the austenitic stainless steels 21Cr–6Ni–9Mn, stable 310 SS [90,91], and unstable 304 SS [90,91]. An example of hydrogen-enhanced shear localization is shown in Fig. 7, in which slip traces as a function of hydrogen content are compared in 310 SS [90] and in the austenitic stainless steel 21Cr–6Ni–9Mn [120]. High-purity Al (99.999% purity), that normally exhibits very fine slip, showed highly localized, coarse shear bands after high-fugacity charging with H (Fig. 2) [121].

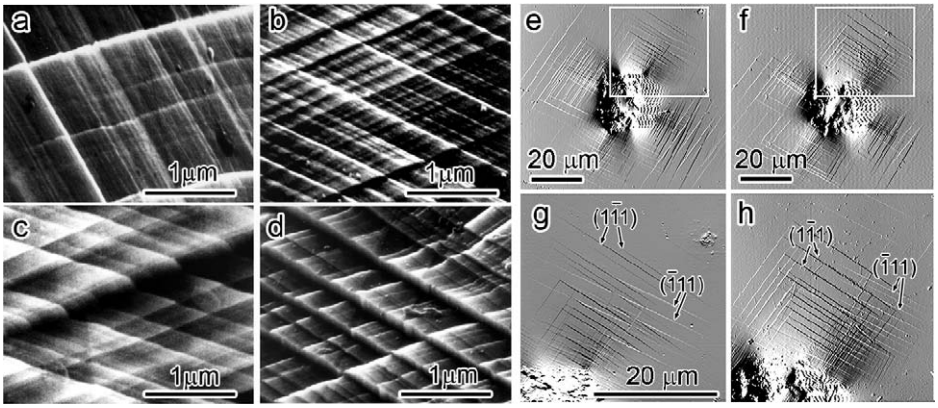

Fig. 7. (a–d) Slip traces on the surface of 310 SS tensile tested to failure at 295 K and a strain rate of $5.5 \times 10^{-5}\,s^{-1}$. (a) H/M = 0.0; (b) H/M = 0.8×10^{-3}; (c) H/M = 1.8×10^{-2}; and (d) H/M = 2.7×10^{-2}. Reprinted from Ref. [90] with permission from Springer. (e–h) Indentations made into a grain with a surface orientation of (018) prior to hydrogen charging (e) as well as after hydrogen charging (f) display slips with a similar general pattern of slip steps. The upper right regions, marked by the box in (e) and (f) are detailed in (g) and (h) and show that the number of slip steps is increased by charging with hydrogen B. Reprinted from Ref. [120] with permission from Elsevier.

In the case of the Al–H system, the shear localization was probably the result of the introduction of gas bubbles during the H charging [87] (Fig. 3). In contrast, a decrease in shear banding has been reported in steels at low H fugacities [122].

3. In situ *TEM studies of dislocation behavior*

A large number of direct observations of the effects of solute H on the behavior of dislocations have been carried out by conducting deformation experiments *in situ* in an environmental cell TEM [123,124]. This method allows observation of dislocation behavior in H_2 gas at a fugacity of up to about 40 MPa [125] while the specimen is being stressed. Studies have been carried out on fcc [37,39,49], bcc [35,36,126], and hcp [40] systems, on pure metals, on alloys [38,42–44,46] and on intermetallic compounds [41], with the observations being independent of the metallic system.

To understand the results of the *in situ* TEM experiments it is essential that the limitations be understood. Although detailed analysis of the dislocation behavior is possible, the stress applied to the specimen or the H/M value in the observed volume cannot be determined. The shape of a typical miniature tensile TEM specimen – an electron transparent region with a wedge-shaped profile within a much thicker region (100×10^{-6} m) – precludes measurement on the local stress in the observation region. The proximity of free surfaces does impact the dislocation mobility and deformation processes and, therefore, the relevance of conclusions drawn from such observations to deformation behavior in bulk specimens must be made cautiously and claims verified by alternate means. However, the conclusions discussed below are believed to be generally characteristic of bulk behavior. This statement is based on the fact that observations have been made in relatively thick specimens ($\sim 1 \times 10^{-6}$ m thickness) using 1 MeV electrons [43] as well as at lower accelerating voltages and these microscopic observations have been coupled to studies in macroscopic specimens. In addition, observations of dislocations and sources moving completely within the volume of the TEM specimens were identical to those made on dislocations that terminated at the surfaces of the specimen.

In the reported environmental cell TEM deformation studies, the specimen tensile rod was designed to maintain a constant load when the displacement applied to the specimen was stopped, i.e., it was designed as a ‘‘soft machine.’’ In some cases, the experiments were carried out in a ‘‘hard’’ tensile rod designed to maintain a constant displacement when the applied displacement rate was decreased to zero. The results in both cases were confirmatory. Although the H_2 pressure in the environmental cell could be measured directly, the actual concentration in the specimen could not be. However, as the specimen thickness was about 100 nm in the regions studied, equilibration with the H_2 gas is expected to take place in less than a second after the gas is introduced into the cell. The fact that the H_2 gas molecules are dissociated and the H is ionized by the electron beam increases the H fugacity and assures that any surface oxides do not provide a barrier to H entry [125]. In some alloy systems [127], an evaporated film of Pd in the vicinity of the

electron transparent regions was used to enhance entry of H [128]. Observations made with H_2 atmospheres were unique to this environment and were not duplicated when an inert gas such as He was added to the cell.

The major observations made with the environmental cell TEM apply to all systems studied and are:

- Introduction of H_2 gas into the environmental cell, while the specimen was under constant applied stress, resulted in increased dislocation velocities. Dislocations that were moving under the stress moved faster and those that were immobile began to move. Removal of the gas resulted in a decrease in dislocation velocity. Reintroduction of the gas to the environmental cell and hence the metal increased the dislocation mobility. The effect of introducing and removing the gas on the dislocation velocity could be repeated provided the stress remained constant. An example of the hydrogen-induced enhancement of the dislocation mobility in Fe is shown in the time-sequence of images presented in Fig. 8; these dislocations were created by deforming the sample in vacuum, the applied load was then held constant and the dislocations allowed to come to rest before hydrogen gas was introduced to the environmental cell. The repeatability of the effect is demonstrated with the first introduction and removal of hydrogen occurring in images Figs 8(a)–8(e); note the similarities in dislocation configurations in images Figs 8(e) and 8(f) which shows the images are stationary. Hydrogen gas was introduced again in Fig. 8(g) and the dislocations begin to move again.
- The relative magnitude of the increase in velocity due to hydrogen can be determined by introducing gas while the dislocations are mobile under an applied load and then recording the change for specific dislocations. Examples of the results of such experiments in Fe [35,126] and α-Ti [40] are presented in Fig. 9.

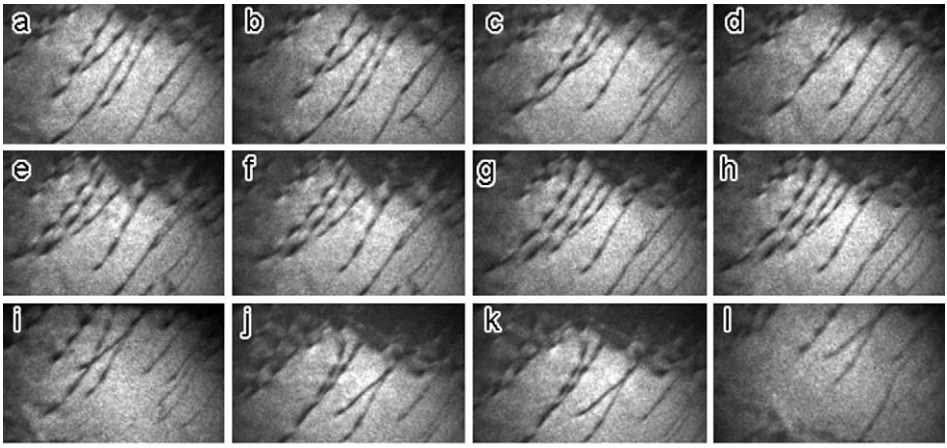

Fig. 8. Hydrogen induced dislocation motion in iron. The time (seconds: hundredths of seconds) of the images is (a) 0, (b) 0:17, (c) 0:90, (d) 2:03, (e) 3:73, (f) 3:84, (g) 14:53, (h) 14:77, (i) 21:29, (j) 21:54, (k) 23:54, and (l) 26:34. (T. Tabata, unpublished work).

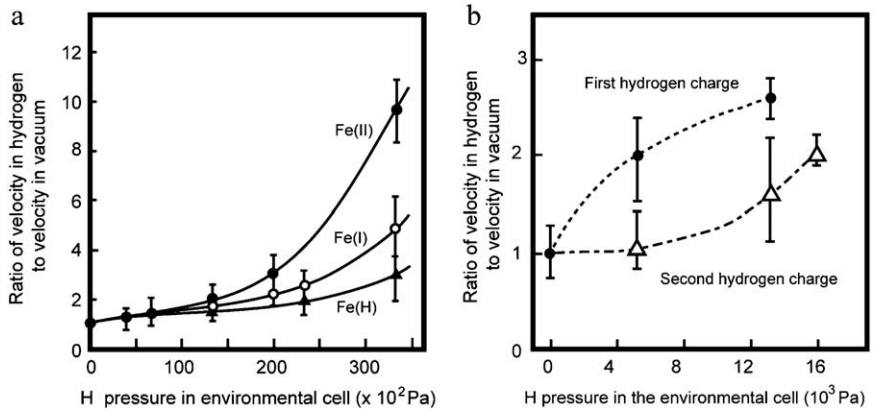

Fig. 9. (a) Ratio of the dislocation velocity in H_2 at the indicated pressures to that in vacuum for Fe of various purities as measured in the environmental cell TEM. Fe(H) is zone refined Fe with a RRR of ~5500. Fe (I) is purified Fe with about 52 appm (C and N). Fe (II) is "pure" iron with about 130 appm (C and N) (Ref. [126]). (b) Ratio of the dislocation velocity in H_2 at the indicated pressures to that in vacuum for α-Ti. Reprinted from Ref. [40] with permission from Elsevier.

Enhancements in velocity of 10 can be achieved even at modest pressures of H_2. The effect of cycling the gas in and out of the environmental cell is shown for α-Ti in Fig. 9b.

- Hydrogen enhancement of the dislocation velocity was independent of material, crystal structure, and dislocation type. It was observed for dislocations moving on the $\{1\,1\,0\}\langle 1\,1\,1\rangle$ and $\{1\,1\,2\}\langle 1\,1\,1\rangle$ slip systems in bcc Fe, on $\{1\,1\,1\}\langle 1\,1\,0\rangle$ systems in fcc metals, and on the $(0\,0\,0\,1)$ and $\{1\,0\,\bar{1}\,0\}$ planes in hcp systems. These effects have been observed for perfect edge, screw and mixed dislocations, for isolated dislocations, for dislocations in tangles, for partial dislocations, and for grain boundary dislocations.
- Dislocation velocity enhancement by H_2 was largest in materials that contained other elastic obstacles such as interstitial solutes. This was particularly evident in Fe [Fig. 9(a)] and in Ni. Experiments on γ'-strengthened Inconel 718 [50] showed extreme enhancement of the dislocation velocity when H_2 was added to the environmental cell. Here the velocity enhancement was sufficiently high to preclude capturing the motion of individual dislocations on the recording medium, which had a time resolution of 1/30th s.
- Enhanced dislocation velocities were reported for H_2 gas and for water-saturated helium gas, but not for dry helium gas [38,39]. These observations confirmed that H and not simply pressure fluctuations were responsible for the enhanced dislocation velocities.
- Dislocation generation rates from sources such as grain boundaries, stress concentrations, etc., were increased by the presence of H_2 gas in the environmental cell and decreased by the return to a vacuum environment.

Data obtained on hydrogen-enhanced dislocation mobility, such as presented in Fig. 9a for Fe–H, can be used to estimate the resultant softening. The plastic strain rate, $\dot{\varepsilon}$, is given by:

$$\dot{\varepsilon} = \rho_m b v_d, \tag{6}$$

where v_d is the average dislocation velocity and ρ_m the mobile dislocation density. Dependence of the dislocation velocity on the resolved shear stress, τ, can be described by:

$$v_d = v_0 \left(\frac{\tau}{\tau_0}\right)^m, \tag{7}$$

where v_0, τ_0, and m are empirical constants. The resistance to dislocation motion is contained in the parameter τ_0 and the stress exponent, $m = 2.6$ [129]. The ratio of the flow stress in H to that in vacuum, τ_H/τ_v, can be calculated from eqs (6) and (7) and the data of Fig. 9(a) (obtained at constant applied stress) with the assumption that ρ_m, v_0, and m are not affected by H solutes. The results from such a calculation are presented in Fig. 10, which shows a softening of about 50% can be obtained in Fe with the low H/M values that are appropriate to the environmental cell TEM experiments.

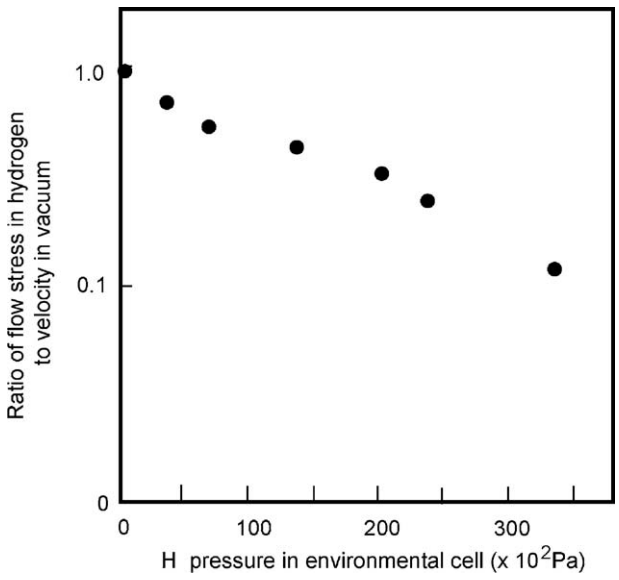

Fig. 10. Calculated ratio of the flow stress in H to that in vacuum using the data of Fig. 6 and eqs (6) and (7).

4. Thermal activation parameters for dislocation motion

At present the direct study of the effects of H on dislocation behavior in bulk specimens is not possible. However, one can use macroscopic methods to determine H effects on the interactions of dislocations with defects that provide barriers to thermally activated dislocation motion [130]. We put forward such studies on high-purity Ni and Ni–C alloys using load relaxation, and temperature and strain rate change techniques [131]. The thermally activated strain rate can be expressed as:

$$\dot{\varepsilon} = \dot{\varepsilon}_0 \exp\left(-\frac{\Delta H_0^* - \int bA^* d\sigma^*}{kT}\right), \tag{8}$$

where the parameter $\dot{\varepsilon}_0$ is given by $\dot{\varepsilon}_0 = v_D \rho_m Ab \exp(\Delta S^*/k)$; v_D, the dislocation attempt frequency in overcoming barriers; A^*, the slip plane area swept by the dislocation per activated event and is a function of the effective stress σ^*, which is equal to the applied stress minus the internal stress opposing dislocation motion; ΔS^*, the activation entropy for slip activation, and ΔH_0^*, the activation enthalpy for slip activation at zero stress. These measured activation parameters are related to the dislocation velocity by:

$$v_d = \frac{\dot{\varepsilon}_0}{\rho_m b} \exp\left(-\frac{\Delta H^*}{KT}\right), \tag{9}$$

where $\Delta H^* = \Delta H_0^* - \int bA^* d\sigma^*$. The critical parameters that control the thermal activation of dislocations over barriers are the activation area, A^*, and the activation enthalpy, ΔH^*.

In the stress relaxation experiments, interstitial C decreased the relaxation rate in Ni and H increased the relaxation rate in both pure Ni and Ni–C alloys [131]. Since the H was introduced from a relatively low-pressure H_2 gaseous atmosphere, the changes in the relaxation rate cannot be attributed to irreversible damage [132]. Using eq. (8) and appropriate variations thereof to analyze the results of stress relaxation, strain rate change, and temperature-change experiments, one can calculate the influence of hydrogen and carbon solutes on the activation parameters. The results of this analysis are shown in Figs 11 and 12. Interstitial C increases A^* and ΔH^* over wide stress ranges consistent with the strengthening effect of C on the flow stress of Ni. Introduction of solute H decreases these activation parameters consistent with interstitial H causing a decrease in the obstacle strength. The softening effect of H is greatest at the lowest stresses at which the thermal activation over barriers dominates dislocation behavior.

The effect of H on the velocity of dislocations can be calculated from this data using eq. (9); the results are presented in Table 3. In this table, σ_a is the applied stress, $\delta\Delta H^*$ is the hydrogen-induced *change* in activation enthalpy, $\delta A^*/b^2$ is the hydrogen-induced *change* in activation area, and v_d^H/v_d is the dislocation velocity in the presence of H relative to that in the absence of H as calculated from the measured dislocation parameters. The values of v_d^H/v_d indicate that very significant enhancement of dislocation velocities are expected in Ni and Ni–C alloys on adding

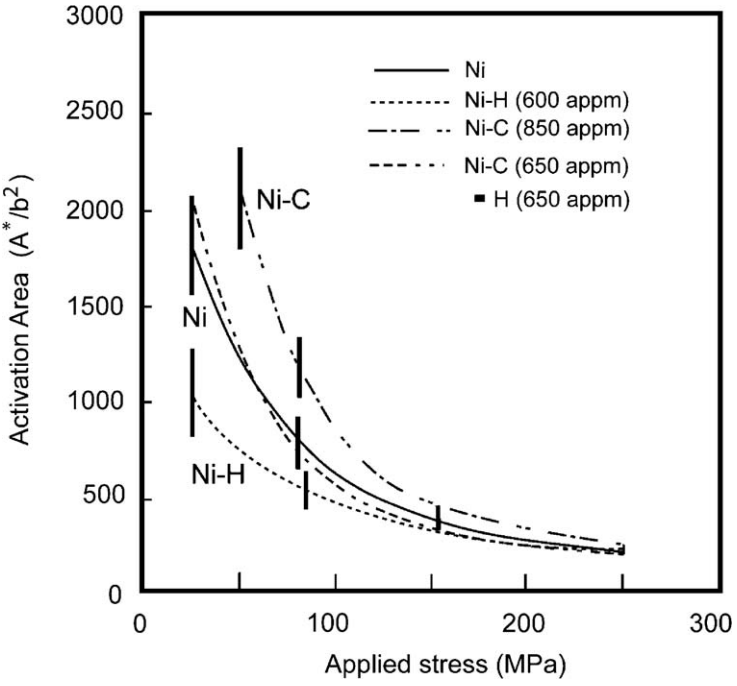

Fig. 11. Dependence of the activation area, A^*, for dislocation motion on the applied stress for pure Ni and for Ni–H, Ni–C, and Ni–C–H alloys. Reprinted from Ref. [131] with permission from Elsevier.

solute H, particularly at the lower applied stresses. These results are consistent with the *in situ* TEM studies in which the stresses, while not directly measured, are expected to be in the range of 100–150 MPa and the measured dislocation velocity enhancements are of the order of 10. The largest amount of softening occurs at the lowest stresses, and hence at the lowest dislocation velocities, suggesting that the effect is dependent upon the motion of H with the dislocations. The significance of this observation is discussed further below. These results were obtained in relatively thick specimens and the agreement with the TEM observations obviates the criticism that the observed enhanced dislocation velocities are ''thin film'' artifacts.

5. Discussion

5.1. Hydrogen effects on dislocation mobility

In the above presentation of the experimental data we showed that the enhanced dislocation velocity due to solute H could be used to estimate a decrease of the flow stress in Fe by about 50%. This estimate was made using eqs (6) and (7), assuming

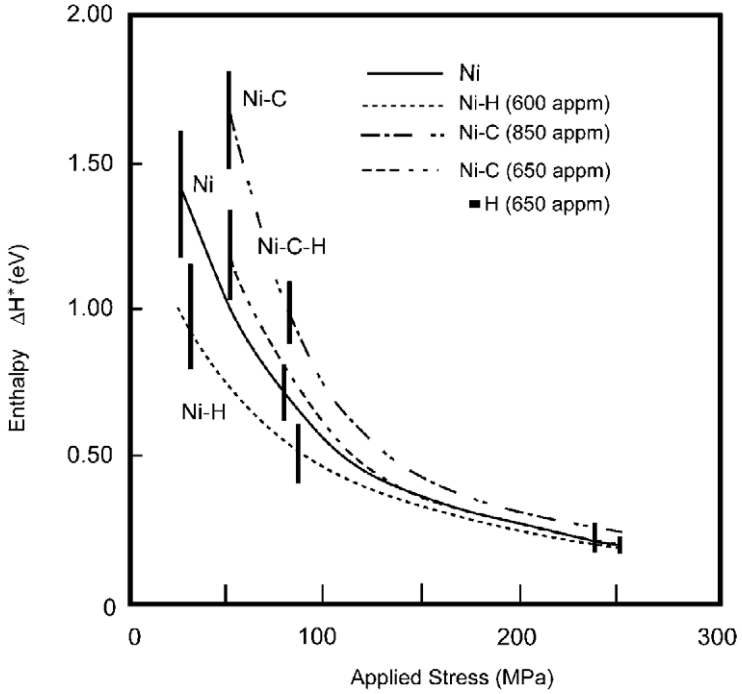

Fig. 12. Dependence of the activation enthalpy, ΔH^*, for dislocation motion on the applied stress for pure Ni and for Ni–H, Ni–C, and Ni–C–H alloys. Reprinted from Ref. [131] with permission from Elsevier.

Table 3
Effect of hydrogen on the activation enthalpy, activation area, and dislocation velocity

	σ_a (MPa)	$\delta\Delta H^*$ (eV)	$\delta A^*/b^2$	v_d^H/v_d
Pure Ni	50	−0.32	−500	3×10^5
Pure Ni	100	−0.11	−200	81
Pure Ni	150	−0.05	−100	7
Ni–C	50	−0.49	−800	3×10^8
Ni–C	100	−0.13	−300	181
Ni–C	150	−0.06	−150	11

that ρ_m, m, and v_0 are independent of H, and that the effect of H is on τ_0 only. This estimate is for the stress range of the *in situ* TEM studies which is restricted by the technique and the time resolution of the camera to dislocation velocities of a few micrometers s^{-1}. Consistent with the TEM experiments, the dislocation activation parameters obtained from the relaxation experiments on Ni show that in both pure Ni and Ni–C alloys, H causes very large increases of dislocation velocities, particularly at low stresses (Table 3).

Although these experiments clearly show that H-enhanced dislocation velocities should give rise to decreases in the flow stress these effects cannot by themselves explain all of the macroscopic deformation experiments. As previously discussed, solute H can cause both softening and hardening of the macroscopic flow stresses. While some of the experimental results can be explained by irreversible damage caused by hydrogen charging, it will be demonstrated below that in the absence of irreversible damage, both macroscopic hardening and softening can be observed due to interstitial H.

5.2. Shear localization

In the stainless steel–H alloys, strain localization was accompanied by significant increases in the flow stress [90,91,133], whereas in the Al–H alloys, significant decreases in the flow stresses were observed [121]. *In situ* environmental cell TEM experiments also showed strain localization when H was added to the cell. Here it is worth noting that shear localization is not a unique phenomenon of hydrogen and is often observed in the deformation microstructure in systems containing precipitates [134] and in irradiated materials [135–138]. In hydrogen-charged steels [113,114], strain localization due to H has been correlated to the carbide precipitates. However, in other systems strain localization caused by H occurs in the absence of any second phases or voids and in such systems the mechanism by which H causes shear localization is not yet established.

It has been suggested that slip planarity is increased when H is added through it decreasing the stacking-fault energy. This effect would increase the equilibrium separation distance of the bounding partial dislocations and thereby increase the force needed to create the constriction necessary for cross slip, making it less probable. A direct test of this idea was carried out by determining the stacking-fault energy in 310 SS from the curvature of dislocation nodes created by deforming samples in the TEM in vacuum and in hydrogen environments [44]. The change in node curvature was consistent with the stacking-fault energy decreasing from $36.9\,\mathrm{mJ\,m^{-2}}$ to $29.7\,\mathrm{mJ\,m^{-2}}$ when H was present. This 20% reduction is smaller than the 40% reduction reported by Pontini and Hermida [139] for a 304 steel; the difference may be related to the experimental techniques – TEM versus X-ray diffraction. Delafosse and coworkers [140–143] have proposed that the change in separation distance between the bounding partial dislocations is not necessarily or entirely attributable to a decrease in the stacking-fault energy but to the screening effect of hydrogen on the edge component of the partial dislocations; this screening mechanism is discussed further in Section 6.3. The impact of the screening effect on the equilibrium separation distance between the bounding partial dislocations and the work required to create the constriction necessary for cross slip is shown for nickel as a function of hydrogen content in Fig. 13; here it was assumed that the stacking-fault energy was independent of hydrogen concentration and constant at $100\,\mathrm{mJ\,m^{-2}}$. An alternative explanation that is more general considers the initial distribution of hydrogen around a mixed character dislocation and the need for

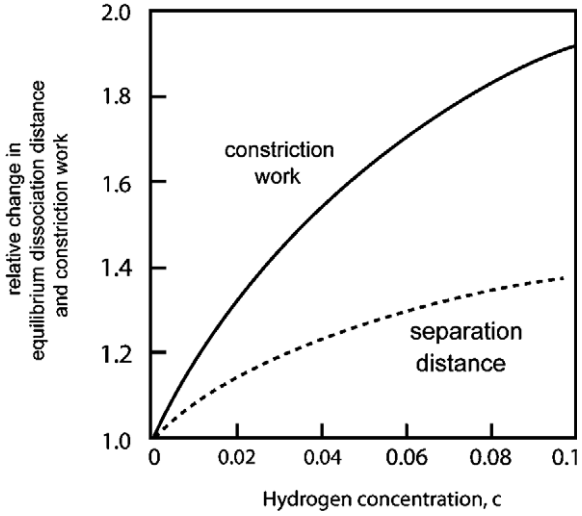

Fig 13. Relative change in equilibrium dissociation distance and work of constriction as a function of hydrogen concentration in nickel at 300 K. Reprinted from Ref. [140] with permission from Elsevier.

redistribution of hydrogen as the dislocation character shifts to pure screw for cross slip [49]. Since there is no driving force to cause the hydrogen to move from the atmosphere to the surrounding lattice, the nonuniform distribution of the hydrogen atmosphere around the dislocation prohibits it from cross slipping. It has yet to be determined which of these mechanisms is operative but what is clear is that the magnitude of the change in the equilibrium separation distance is unlikely to be of sufficient magnitude to have a profound effect on the ability of the dislocations to cross slip.

The effects of strain localization caused by H on the increases or decreases of the macroscopic tensile flow stress can however be understood [144]. Clearly, the flow stress in the region of localization is reduced relative to the flow stress of the nondeforming volume (this is by definition shear localization). The effect of hydrogen-related decreases in the stress to move dislocations and shear localization can be to increase or decrease the measured macroscopic flow stress measured in a tensile test. This may account for the disparity of softening and hardening observations due to H in various experiments. We can distinguish three cases where H-caused shear localization occurs.

- Case I. In systems where H *reduces* the barriers to dislocation motion, an inhomogeneous distribution of H can cause shear localization, since the flow stress is lower where the H concentration is greatest. This may occur if H entry is facilitated at slip-line intersections with the surface and may be what occurs in front of propagating cracks.
- Case II. Shear localization can also occur when the specimen is *hardened* by the introduction of hydrogen (due to the formation of hydrides or H clusters), if the

initial deformation locally reduces the stress for continued slip, e.g., by "cutting" through the hydrides. Removal of these clusters during the initial passage of dislocations leads to slip localization, as in other precipitation hardened systems. A related situation is when gas bubbles are formed during charging.

- Case III. Shear localization can occur in systems with a uniform hydrogen distribution, no stress concentrators and no second phases through the hydrogen-induced volume dilatation effect [145].

Relating the imposed displacement rate to the plastic strain rate in a macroscopic test such as a tensile test generally is based on the assumption that slip occurs uniformly over the gage length, l_u. This assumption is inappropriate when shear localization occurs. With localization, slip is confined to those regions in which dislocations are active and the sum of these localized portions of the gage length then comprise the active gage length, l_l. The imposed macroscopic displacement rate, $\dot{u}$, is the same regardless of the degree of slip localization and is given by the condition:

$$\dot{u} = l_u(\dot{\varepsilon})_{\text{unlocalized}} = l_l(\dot{\varepsilon})_{\text{localized}}. \tag{10}$$

The effect of H is threefold – (1) shear localization is induced, (2) the velocity of the dislocations is increased at each stress level, and (3) the number of mobile dislocations is increased. Condition 10 can be combined with eqs (6) and (7) to yield:

$$\frac{l_v}{l_H} = \frac{\rho_{mH} v_{oH} (\tau_H/\tau_{oH})^{m_H}}{\rho_{mv} v_{ov} (\tau_v/\tau_{ov})^{m_v}}. \tag{11}$$

Here the subscripts v and H denote deformation in vacuum (a relatively uniform distribution of slip along the gage length, $l_v = l_H$) and in H-charged specimens (localized shear, $l_l = l_H$). The mobile dislocation densities are given by ρ_{mv} and ρ_{mH}, m_v and m_H are the stress exponents, v_{ov} and v_{oH} and τ_{ov} and τ_{oH} are the corresponding constants in eq. (7). The stresses required for the imposed displacement rate in the two cases are τ_v and τ_H. The number of parameters in eq. (11) is too large to permit evaluation through analysis of the available data set. However, since the experimental observations indicate that the effect of H on dislocation behavior is to reduce the strength of obstacles to dislocation motion, a reasonable assumption is that solute H affects primarily τ_0 leading to:

$$\frac{\tau_H}{\tau_v} = \left(\frac{l_v}{l_H}\right)^{1/m} \left(\frac{\tau_{oH}}{\tau_{ov}}\right). \tag{12}$$

Thus measurement of the effects of H on the macroscopic flow stress alone is not a reliable means of determining dislocation behavior. In the general case, as localization occurs, the plastic strain rate in the active slip regions must increase to meet the imposed $\dot{u}$ and this normally would result in an increased flow stress [eqs (6) and (7)]. However, localization caused by solute H is accompanied by a decrease in the stress to move dislocations, an increased dislocation velocity at the

imposed stress, and an increase in the dislocation density in the active shear regions. Thus, as seen in eq. (12), this can lead to a decrease of τ_H/τ_v, i.e., a *decrease* in the flow stress. Increases in the flow stress due to the introduction of H may result from shear localization if the *increased* dislocation mobility due to H does not balance the shear localization.

5.3. Elastic shielding of stress centers

The H-caused increases in the dislocation velocity and the related flow stress changes were observed in fcc, bcc, and hcp systems, in pure metals, solid solutions, and in precipitation hardened systems. Its cause lies in the elastic interactions between dislocations and other stress centers, such as solute atoms and precipitates. The primary interaction between the stress centers, such as dislocations, and H is the elastic interaction energy, $W_{int} = W^{(1)}_{int} + W^{(2)}_{int}$ [146], which is expressed as the sum of the first-order dilatational interaction energy and the second-order modulus-related interaction energy. The first-order dilatational interaction energy $W^{(1)}_{int}$ can be expressed as:

$$W^{(1)}_{int} = -\frac{1}{3}\sigma^a_{kk}\Delta v, \tag{13}$$

where σ^a_{kk} is the hydrostatic stress field of a defect and Δv is the unconstrained volume dilatation of the H solute. The second-order H-defect interaction energy, $W^{(2)}_{int}$, derives from the H-induced modulus change and can be expressed as:

$$W^{(2)}_{int} = \frac{1}{2}\varepsilon'_{ij}\varepsilon^a_{kl}v_s(C'_{ijkl} - C_{ijkl}). \tag{14}$$

In eq. (14) v_s is the volume over which the solute atoms alter the elastic stiffness C_{ijkl}, ε^a_{ij} are strains caused by the applied stress σ^a_{ij} in the absence of the solute atoms, ε'_{ij} are elastic strains inside the volume v_s after the solute atom has been introduced in the lattice in the presence of the applied stresses which are held constant. The primed stiffnesses correspond to those characteristic of the local stiffness in the presence of the solute atoms. These interactions give rise to H atmospheres around edge dislocations ($W^{(1)}_{int}$ and $W^{(2)}_{int}$), screw dislocations ($W^{(2)}_{int}$), and point defects ($W^{(1)}_{int}$and $W^{(2)}_{int}$). Since the local hydrogen concentration at each point in the stress field of every defect responds to the total stress at that point, the local H concentration at two interacting defects responds to the sum of the stresses due to all defects [147]. As the defects move relative to each other, the mobile H solutes respond and the H atmospheres act to minimize the total energy of the system, i.e., the H solute atmospheres act to shield the elastic interactions. Hydrogen atmospheres, treated as a set of cylindrical dilatational centers with a radial expansion of εr_0 and with the axis of their cylinders parallel to the length of the dislocation, generate stresses described by:

$$\sigma_{rr} = -\frac{\mu\Delta a}{\pi r^2}, \quad \sigma_{\phi\phi} = \frac{\mu\Delta a}{\pi r^2}. \tag{15}$$

where $\Delta a = \pi r_o \varepsilon/(1-\nu) = V_H/2N_A(1-\nu)h$, μ is the shear modulus of the material, r, ϕ, and x_3 are the polar coordinates of the H dilatational cylinder with x_3 parallel to the dislocation, N_A the Avagadro's number, and h the distance between H atoms in the dilatational cylinder. The interaction energy per unit length of this H cylinder with a stress field σ_{ij}^a is:

$$W_{\text{int}}^{(1)} = -\frac{\sigma_{11}^a + \sigma_{22}^a}{2}\frac{V_H}{N_A}. \tag{16}$$

If there are multiple sources of stress, e.g., the presence of several dislocations, the $W_{\text{int}}^{(1)}$ is determined from a linear superposition of the stresses. It is this interaction energy that determines the H/M at every point in the stress field. Setting $\Delta E = -W_{\text{int}}^{(1)}$ and $\theta_L = c_0/\beta$ in eq. (16) with c_0 being the nominal concentration in the absence of the defect, we calculate the hydrogen concentration as $C = \beta N_L \theta_T$ measured in H atoms per unit volume. Since the stress field of the H solute is purely deviatoric, the interaction between the H cylinders is zero, however, the shear stress field of the H does cause a force on an adjacent dislocation. In the case of the two parallel edge dislocations 1 and 2 shown in the inset of Fig. 16, the shear stress due to H at the core of dislocation 2 resolved along the slip plane is given by:

$$\tau_H = -\frac{\mu}{2\pi(1-\nu)}\frac{V_H}{N_A}\int_0^{2\pi}\int_{r_0}^{R} C(r,\phi)\frac{\sin 2\phi}{r}\mathrm{d}r\mathrm{d}\phi, \tag{17}$$

where r_0 is the inner cutoff radius of dislocation 2 and R is the outer cutoff radius of the atmosphere centered at the core of dislocation 2. The problem of the interaction between dislocations with hydrogen atmospheres was solved using the above relations and the application of both analytic and finite element solutions – with excellent agreement between the two methods [146–147].

All of the calculations corresponded to an equilibrium distribution of H atoms. Some results from these calculations are shown in Figs 14 and 15. Fig. 14(a) [147] shows the isoconcentration contours for H around an isolated edge dislocation in Nb (for which the required data set is most complete) and Fig. 14(b) [140] for a dissociated dislocation in nickel. These isoconcentration plots show that in cases for which the first-order interaction dominates, hydrogen is accumulated in the tensile side of an edge dislocation and for the partial dislocation the distribution is biased toward the edge component. The distribution, shape, and isoconcentration lines, of hydrogen are modified in the presence of another elastic obstacle. Fig. 15 shows the changes in the shape and concentrations that occur when a second identical edge dislocation is positioned coplanar and proximal to the first. Changes in the H concentrations are due to the presence of the stress fields of both dislocations interacting with the H. Integrating the forces on the dislocations due to the entire H distribution allows calculation of the effect of the solute atmosphere on the interactions between the two parallel dislocations. These results are shown in Fig. 16 for the shear stress on dislocation 2 due to the presence of dislocation 1 and the H atmospheres. In the absence of the atmosphere, the normalized shear stress, τ/μ, shows the expected $(l/b)^{-1}$ dependence with separation distance l along the slip

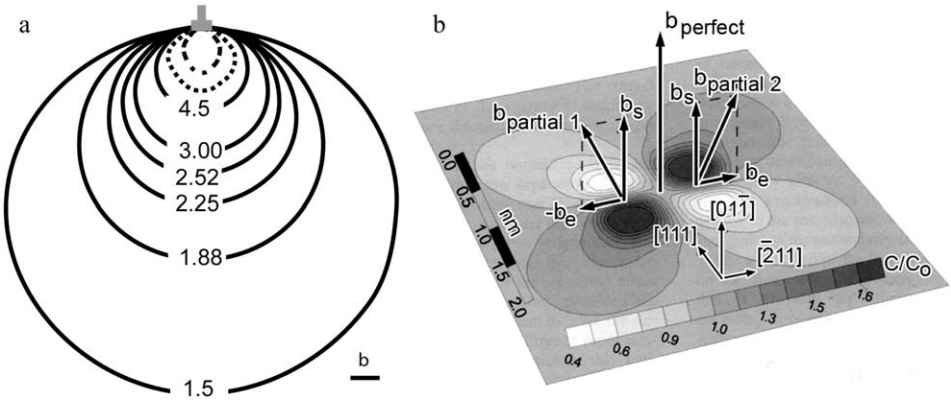

Fig. 14. Contours of the normalized H concentrations, c/c_o, around: (a) An isolated edge dislocation in Nb. The average concentration in the lattice is c_o = H/Nb = 0.1 and the temperature is 300 K. Reprinted from Ref. [147] with permission from Elsevier. (b) A dissociated screw dislocation in Ni. Reprinted from Ref. [140] with permission from Elsevier.

plane. As shown in Fig. 16 the H atmospheres provide an attractive force that varies as $(l/b)^{-2}$ and decreases the repulsion between the dislocations. In effect, H ''shields'' the elastic interaction between the dislocations. Here it is important to note that the asymmetric distribution of hydrogen around an edge dislocation introduces a directional dependence to the effect of hydrogen on the stress-field distribution. For example, the normal stress associated with a dislocation array will actually be increased in the presence of hydrogen atmospheres and this will impact interactions with dislocations on other slip systems.

Calculations using this methodology were carried out for the interactions between solutes and edge and screw dislocations in the presence of H atmospheres [147]. Some examples of these results are shown in Figs 17 and 18. For the case of dislocations interacting with interstitial C solutes, the results of the finite element calculations in the absence of H agreed very well with the analytic solutions of Cochardt et al. [148]. As an edge dislocation moves past a C atom lying close to the slip plane ($x_2/b = -0.505$) (Fig. 17) it experiences an interaction energy of –1.1 eV per distance ''a'' along the dislocation line, a being the lattice parameter. Adding H at a concentration of H/M = 0.1 decreases the interaction energy, i.e., H shields the elastic interaction. The first-order volumetric interaction is relatively small – a decrease of the interaction energy of about 0.14 eV – whereas the decrease due to the volumetric and the second-order modulus effect is much larger – a decrease of the interaction energy of about 0.48 eV. Also shown is a calculation for the edge dislocation based on the formalism of Larche and Cahn [149] that accounts for the modulus change but assumes a uniform distribution of H. As seen in Fig. 17, elastic shielding due to H causes a very significant decrease in the interaction energies between an edge dislocation and an elastic pinning point such as a C interstitial. The shielding effect would be applicable for the interaction of edge dislocations with any elastic center. As seen in Fig. 17, the width of the interaction curve is also

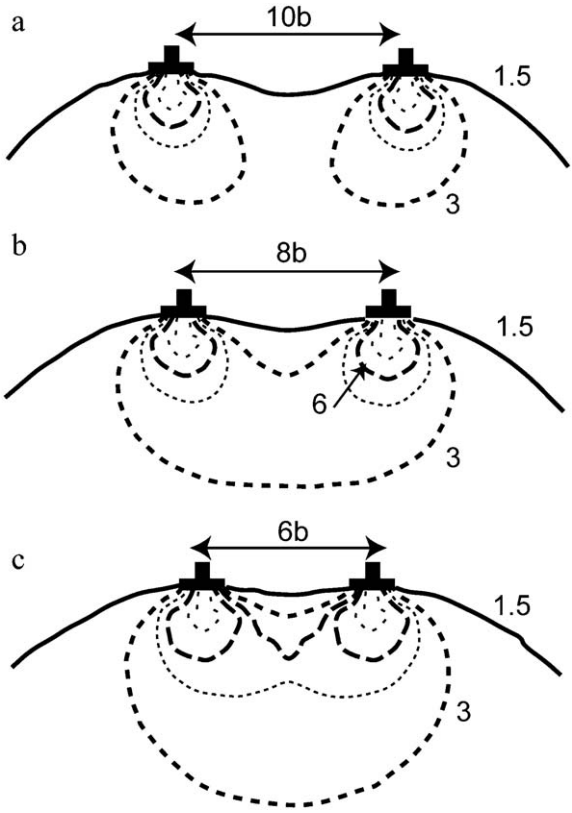

Fig. 15. Contours of the normalized H concentrations, c/c_o, around two parallel edge dislocation having the same Burgers vectors. The average concentration in the lattice is $c_o = H/Nb = 0.1$ and the temperature is 300 K. The parameters used in the calculation are those suitable for the Nb–H system. The grid lines are at distances equal to the Burgers vector. Separation of the edge dislocations are (a) 10b, (b) 8b, (c) 6b. Reprinted from Ref. [147] with permission from Elsevier.

decreased, an effect that is equivalent to a decrease in the activation area, A^*. These results are in agreement with the determination of the effect of H on the thermal activation parameters for dislocations [131] (see Figs 12 and 13).

These effects are somewhat more complex for the elastic shielding of screw dislocations [147] and these studies are ongoing. The effects are considerably smaller than for edge dislocations as the interaction is solely due to the second-order modulus change effect and hence the H concentrations in the screw dislocation atmospheres are very small. Nonetheless, elastic shielding by H does decrease the barriers provided by interstitial solutes such as C to the motion of screw dislocations (Fig. 18).

Elastic shielding of interacting stress centers by hydrogen provides a very natural explanation for the wide variety of observations made using the environmental cell TEM technique. The increase in dislocation velocity on adding H is a direct result of

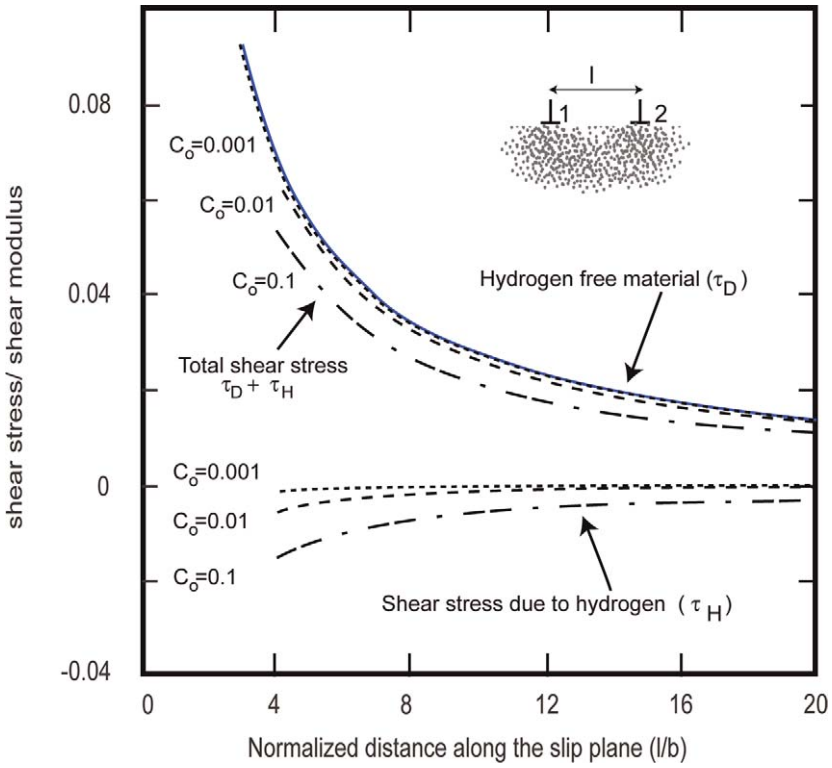

Fig. 16. The normalized shear stress, τ_H/μ, due to the H atmospheres, τ_D/μ, due to dislocation 1, and the net shear stress, $(\tau_H+\tau_D)/\mu$, at the core of dislocation 2 along the slip plane versus the normalized distance between the dislocations, l/b, at a temperature of 300 K and H/Nb = 0.1, 0.01, and 0.001. The dislocation Burgers vectors are of the same sign. Reprinted from Ref. [147] with permission from Elsevier.

decreasing the effectiveness of elastic interactions between the moving dislocations and nearby stress centers, such as other dislocations and solute pinning points, by elastic shielding due to H. The fact that the increased dislocation velocities due to H is most prevalent in systems that have immobile interstitials acting as dislocation barriers (Fig. 10) is consistent with the decrease in the interaction energy by elastic shielding (Figs 17 and 18). Since the concept of elastic shielding is applicable to all crystal systems and in alloys as well as pure materials, this offers a natural explanation for the enhanced velocity observations in a wide range of systems. The reversibility of the enhanced velocity on adding and removing H [45] is also in agreement with the expectations of the elastic shielding model.

The H-shielding model makes several predictions about the behavior of dislocations in the presence of hydrogen. For example, it predicts that the equilibrium spacing between dislocations in the pileup should be less in the presence than in the absence of hydrogen. Although as noted by Chateau et al. [140] this change in spacing does not necessitate an increase in the stress concentration at the head of the dislocation pileup. This prediction was verified by Ferreira

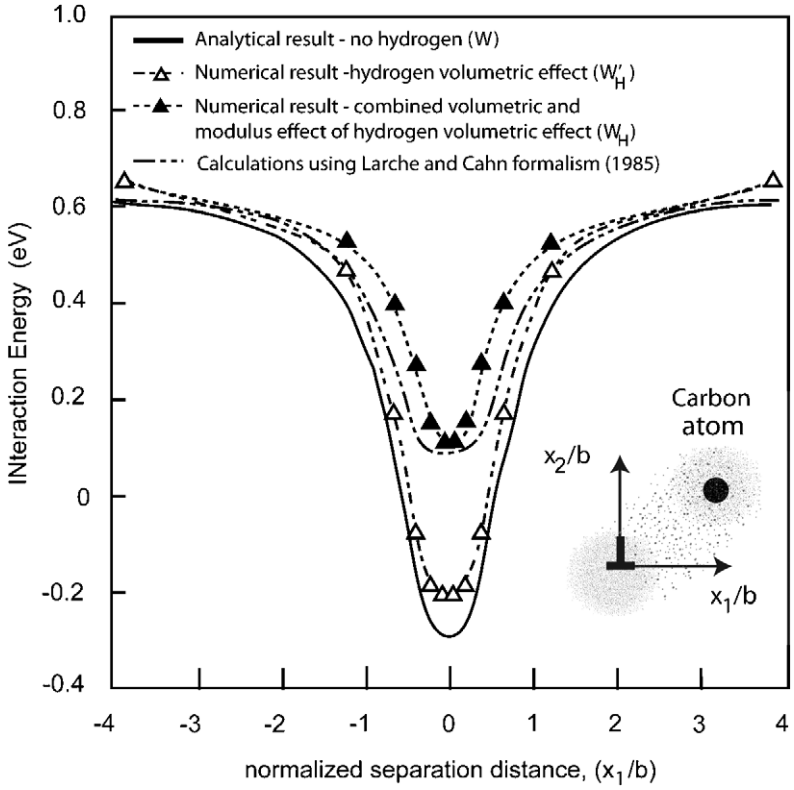

Fig. 17. Plot of the interaction energy for an edge dislocation with a C solute in a bcc metal as a function of the normalized dislocation position, x_1/b, for a C atom lying $x_2/b = -0.505$ below the slip plane and having its tetragonal axis along the [1 0 0]. This calculation is at 300 K and H/Nb = 0.1. H-shielding results are shown for the volumetric and for the volumetric and modulus interactions (Ref. [147]) as well as for the Larche' and Cahn formalism. (Ref. [149]). Reprinted from Ref. [147] with permission from Elsevier.

et al. [49] who showed that the spacing between dislocations in pileups in 310 stainless steel and in 99.999% pure Al decreased when hydrogen was introduced to the material. The increased density in the pileup indicates a decrease in the repulsive elastic interactions between dislocations due to elastic shielding caused by H. An example of this effect in 310 SS is shown in Fig. 19, which is a composite image created by superimposing a negative image of a dislocation pileup (the dislocations appear white) in hydrogen on the positions in vacuum (dislocations appear black). Clearly, all dislocations have moved closer to the obstacle and the separation distance between the dislocations has decreased. This latter effect is quantified for different gas pressures in Fig. 19(b). In the case of Al, this decrease was reversible on removal of the H, while in 310 SS there was a hysteresis in the motion, suggesting strong pinning of the dislocations. The fact that H atmospheres can affect the relative energies of edge and screw dislocation components by the formation of strong H atmospheres at the edge and weak atmospheres at the screw

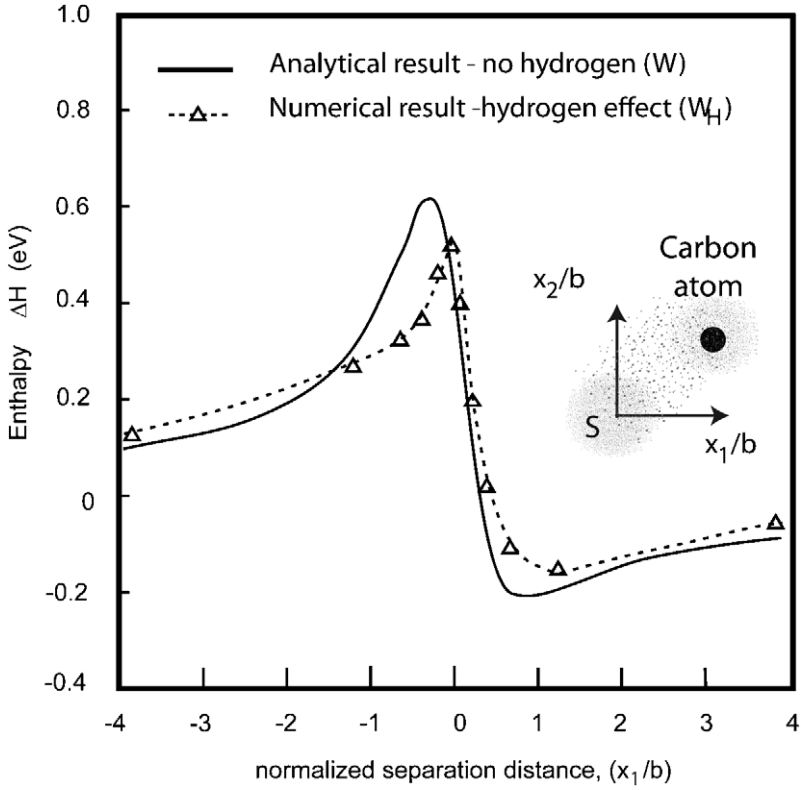

Fig. 18. Plot of the interaction energy for a screw dislocation with a C solute in a bcc metal as a function of the normalized dislocation position, x_1/b, for a C atom lying $x_2/b = -0.505$ below the slip plane and having its tetragonal axis along the [0 1 0]. This calculation is at 300 K and H/Nb = 0.1. H shielding results from the modulus interaction. Reprinted from Ref. [147] with permission from Elsevier.

components was also shown by a study of the cross slip of dislocations in Al using the environmental cell TEM [150]. Introduction of H_2 gas during the cross slip process stabilized the edge components relative to the screw components and stopped the cross slip process. Removal of the H_2 allowed cross slip to continue. This provides an intrinsic effect that prohibits cross slip from occurring.

5.4. Temperature and strain rate effects

The response of dislocations to the presence of H atmospheres is dependent on the temperature and strain rate. For binding enthalpies (ΔE) of H to dislocations (see Table 2) of 0.1 eV (Ni) and 0.62 eV (Fe) the H concentrations at the dislocations are enhanced relative to the concentration in the lattice [eq. (3)] by factors given by $\exp(\Delta E/kT)$ as shown in Table 4. At these high concentrations, the dislocation

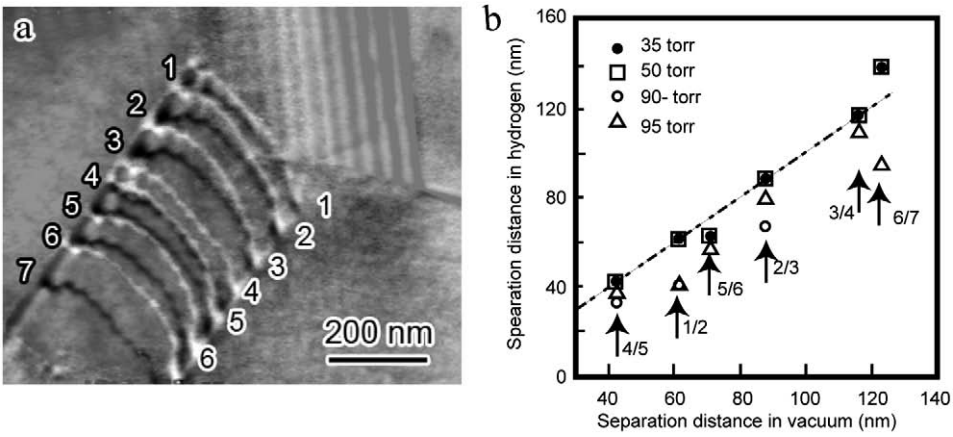

Fig. 19. (a) Effect of internal hydrogen on the dislocation separation distance in 310 SS. The black dislocations show the position in vacuum and the white dislocations the positions in a hydrogen environment. (b) The relative change in position as a function of hydrogen. Reprinted from Ref. [49] with permission from Elsevier.

Table 4
Parameters describing dislocation breakaway

Temp.	Nickel			Iron		
	Dislocation atmosphere (H/M)[a]	D ($m^2 s^{-1}$)	ε_c (s^{-1})	Dislocation atmosphere (H/M)[a]	D ($m^2 s^{-1}$)	ε_c (s^{-1})
100	1.0	4.5×10^{-28}	1.5×10^{-18}	1.0	7.7×10^{-11}	2.6×10^{-1}
200	3.3×10^{-2}	1.8×10^{-17}	1.2×10^{-7}	1.0	4.4×10^{-9}	2.9×10^{-1}
300	4.8×10^{-3}	6.0×10^{-14}	6.2×10^{-4}	1.0	1.6×10^{-8}	1.7×10^{-2}
400	1.8×10^{-3}	3.5×10^{-12}	4.8×10^{-2}	1.0	3.1×10^{-8}	4.3×10^{-2}
500	1.0×10^{-3}	4.0×10^{11}	0.69	1.0	4.7×10^{-8}	8.0×10^{-2}
600	6.9×10^{-4}	2.0×10^{-10}	4.2	3.3×10^{-1}	6.1×10^{-8}	1.3×10^{-3}

[a]Values of H/M = 1.0 in the dislocation atmosphere indicate a saturated atmosphere with Fermi-Dirac statistics.

atmospheres follow Fermi–Dirac statistics as all interstitial sites close to the dislocation are occupied. Also shown in Table 4 is the H diffusivity for these two metals and the calculated critical strain rate, $\dot{\varepsilon}_c$, for breakaway of the dislocations from the H atmospheres as a function of temperature [eq. (5)].

The results of these calculations are also presented graphically in Figs 20 and 21. Hydrogen effects on the flow stress can be observed over the temperature range where significant H atmospheres are present at the dislocations and the mobility of H allows the atmospheres to move with the dislocations at the rate determined by the strain rate. Between these two limits, elastic shielding of the interaction of dislocations with obstacles can decrease the flow stress in the absence of excessive localization.

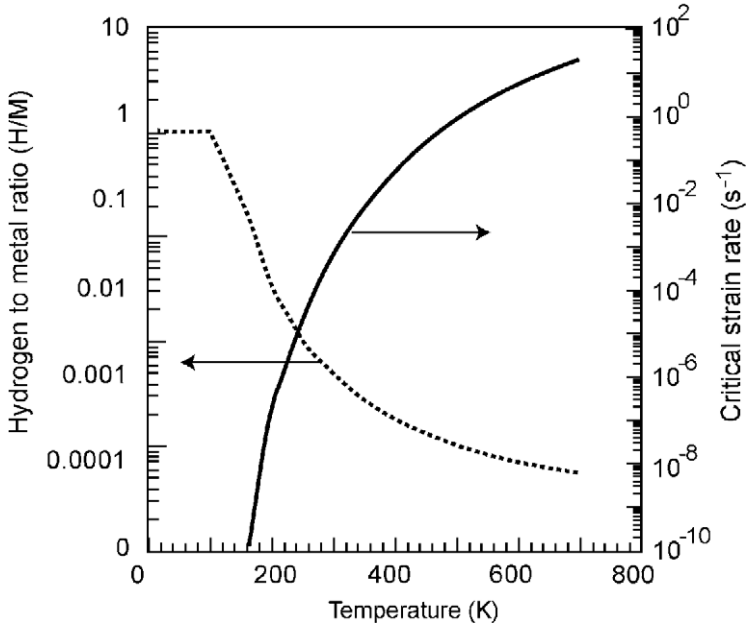

Fig. 20. Concentration of H in the dislocation atmosphere and the critical breakaway strain rate for breakaway of the dislocation from the H atmosphere as a function of temperature for Fe with $H/M = 2 \times 10^{-6}$.

As seen in Table 4 and Fig. 20, the high binding enthalpy for Fe allows it to have a significant H atmosphere over the temperature range 50–600 K with a Fermi–Dirac distribution below about 500 K. The high H diffusivity over the temperature range above 50 K allows the H atmosphere to move with the dislocations at reasonable tensile strain rates. Over the entire temperature range of interest, this high diffusivity and high binding enthalpy to the dislocations results in very high breakaway strain rates. Based on these calculations, H in Fe should result in enhanced dislocation velocities over the range 50–600 K. This situation would be markedly changed if the dislocation trapping enthalpy was significantly reduced or the presence of solute traps decreased the H diffusivity [eq. (2)]. Steels, having significantly reduced H diffusivities due to trapping [17], would not have H atmospheres that could move with the dislocations at low temperatures. Hence, the breakaway strain rates for steels would be greatly decreased at lower temperatures, and particularly at temperatures below 300 K. In high-purity Fe, H atmospheres can move with the dislocations over the entire temperature range 50–600 K and hence should decrease the flow stress over the same temperature range by the H-shielding effect discussed above. This is consistent with the observations by Kimura et al. of decreases in the flow stress on adding H to high-purity Fe in the absence of structural damage [17]. The increases in flow stress they observed below 190 K may be due to the formation of H_2 bubbles during the low-temperature charging that

may act as dislocation barriers. The hardening due to the barriers would be superimposed on the inherent softening due to H in solid solution. Alternatively, this low temperature hardening may reflect a decrease in the H diffusivity due to the remaining solute traps and hence a decrease in the ability of the atmospheres to move with the dislocations.

For fcc systems, where the interaction enthalpy between dislocations and H is of the order of 0.1 eV and the H diffusivities are not as large as in Fe, the case of the Ni–H system (Table 4 and Fig. 21) is "typical." Significant H atmospheres are present below about 500 K. At $\dot{\varepsilon} = 10^{-6}\ s^{-1}$ the atmosphere can move with the dislocations above about 225 K. Below 225 K hardening and serrated yielding is expected as a result of the lagging of the atmospheres behind the dislocations and the "breaking" away of the dislocations from the atmospheres as is observed [108]. At a strain rate of $10^{-6}\ s^{-1}$ decreases in the flow stress may be expected between about 225 and 500 K due to elastic shielding. Again, these behaviors can be affected by the formation of dislocation core "hydrides" [108] and shear localization (see above). Strain rate effects on the H-related decreases in the flow stress are seen in the results on the Ni–C system [47] (Figs 5 and 6) in which a decrease in the flow stress is seen at $\dot{\varepsilon} = 10^{-7}\ s^{-1}$ but not at $\dot{\varepsilon} = 10^{-5}\ s^{-1}$. In this case, the diffusivity D is expected to be significantly reduced by trapping at the C solutes. Since the critical strain rate for breakaway is linearly proportional to D [eq. (5)] the curve for the

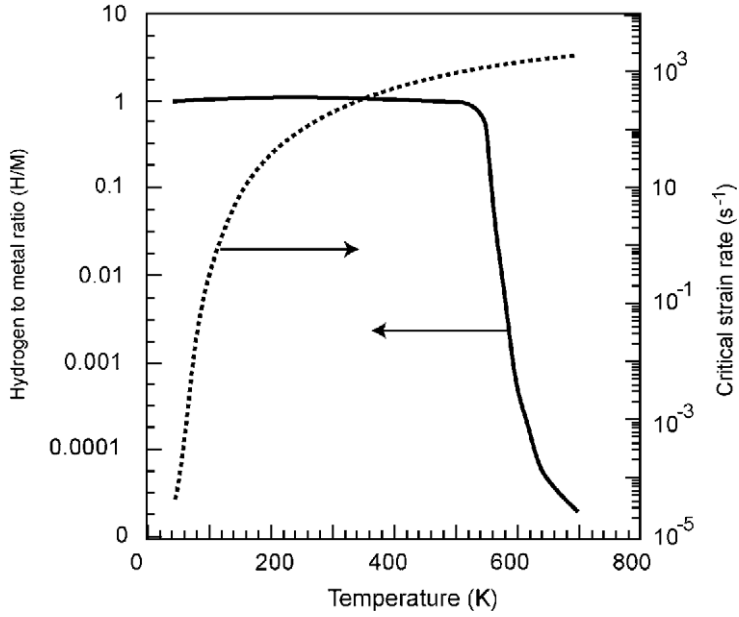

Fig. 21. Concentration of H in the dislocation atmosphere and the critical breakaway strain rate for breakaway of the dislocation from the H atmosphere as a function of temperature for Ni with $H/M = 10^{-4}$.

critical strain rate in Fig. 21 is shifted downwards by an amount equal to the decrease in diffusivity at each temperature.

6. Summary

The effects of H on the plastic properties of metals is dependent upon many factors, chief among which are: (a) the manner in which H is added to the system, (b) the concentration of H, (c) the strain rate of the test, (d) the temperature of the test, (e) the ability or inability of the system to form ''hydrides'' or other second phases, and (f) the H diffusivity and the presence of traps that affect the diffusivity. Introduction of H from a high-fugacity source can cause formation of H_2 bubbles or a high H concentration gradient in the near surface region with the concomitant increase of near surface dislocation density and the injection of dislocations into the solid or formation of near surface phase transitions. The effects can be summarized as follows:

- Formation of large H_2 bubbles causes a decrease in the flow stress due to the decreased cross section of the specimen as well as shear localization.
- Formation of small H_2 bubbles can cause increases in the flow stress due to pinning of dislocations. Similarly, the formation of a high near surface dislocation density, a surface ''hydride layer'' or near surface martensitic phases (in unstable stainless steels) can cause increases in the flow stress.
- Charging of H during deformation can result in the injection of dislocations from hydrides or from the concentration gradients in the near surface regions. These effects can result in decreases in the flow stress.
- Measurements made at ''high'' strain rates (''high'' as measured by the H diffusivity and by the ability of the H solutes to move with the dislocations) tend to result in increased flow stresses. Decreases in the flow stresses are generally observed at low strain rates.
- Solute H increases the mobility of edge, screw and mixed dislocations in fcc, bcc, and hcp systems as long as the H atmospheres can move with the dislocations. Consequently, solute H causes an intrinsic decrease in the flow stress over much of the temperature range of interest and at low strain rates.
- Hydrogen can cause shear localization when it is present as a second-phase hydride and when it is in solid solution. Strain localization tends to increase the macroscopic flow stress. Whether a macroscopic measurement exhibits a decreased or increased flow stress depends on whether or not the hardening due to shear localization exceeds the softening due to increased dislocation mobility.
- The increased mobility of dislocations caused by solute H can be explained on the basis of a theory of ''elastic shielding'' of the interactions between the dislocation and other elastic stress centers.

- Calculations made using the concept of ‘‘elastic shielding’’ are in general agreement with measurements of the parameters that describe dislocation interactions with elastic pinning points, e.g., C and with other dislocations.

Acknowledgments

The authors acknowledge support from (a) the U.S. Department of Energy Grant GO15045; and (b) National Science Foundation Grant DMR 0302470. They also acknowledge the major contributions made by their students, research associates, and colleagues over the many years that this research has been carried out.

References

[1] H.K. Birnbaum, I.M. Robertson, P. Sofronis, D. Teter, in: T. Magnin (Ed.), Corrosion Deformation Interactions CDI’96, The Institute of Materials, Great Britain, 1997, pp. 172–195.
[2] J.P. Hirth, Metall. Trans. A 11A (1980) 861–890.
[3] T. Schober, H. Wenzl, The Systems NbH(D), TaH(D), VH(D): Structures, Phase Diagrams, Morphologies, Methods of Preparation. Hydrogen in Metals. II. Application-Oriented Properties, Springer-Verlag, Berlin, West Germany, 1978, pp. 11–71.
[4] T.J. Udovic, J.J. Rush, R. Hempelmann, D. Richter, J. Alloys Compd. 231 (1995) 144–146.
[5] T. B. Flanagan, W. A. Oates, Ann. Rev. of Mater. Sci. 21 (1991) 269–304.
[6] U. Stuhr, D. Steinbinder, H. Wipf, B. Frick, Z. Phys. Chem. (Germany) 181, 1993, 89–93.
[7] S.A. Danilkin, H. Fuess, H. Wipf, A. Ivanov, V.G. Gavriljuk, D. Delafosse, T. Magnin, Europhys. Lett. 63 (2003) 69–75.
[8] D. Khatamian, C. Stassis, B.J. Beudry, Phys. Rev. B 23 (1981) 624–627.
[9] H. Pinto, H. Shaked, C. Korn, S. Goren, Solid State Commun. 32 (1979) 397–398.
[10] P.P. Narang, G.L. Paul, K.N.R. Taylor, J. Less-Common Metals 56 (1977) 125–128.
[11] G. Bauer, E. Seitz, H. Horner, W. Schmatz, Solid State Commun. 17 (1975) 161–165.
[12] H. Peisl, Lattice Strains Due to Hydrogen in Metals. Hydrogen in Metals I, Springer-Verlag, Berlin, West Germany, 1978, pp. 53–74.
[13] H. Metzger, H. Peisl, J. Phys. F (Metal Phys.) 8 (1978) 391–402.
[14] A. Magerl, B. Berre, G. Alefeld, Phys. Status Solidi A 36 (1976) 161–171.
[15] F.M. Mazzolai, H.K. Birnbaum, J. Phys. F (Metal Phys.) 15 (1985) 525–542.
[16] T. Springer, Investigation of Vibrations in Metal Hydrides by Neutron Spectroscopy. Hydrogen in Metals I, Springer-Verlag, Berlin, West Germany, 1978, pp. 75–100.
[17] J. Volkl, G. Alefeld, Diffusion of Hydrogen in Metals. Hydrogen in Metals I, Springer-Verlag, Berlin, West Germany, 1978, pp. 321–348.
[18] K.W. Kehr, Theory of the Diffusion of Hydrogen in Metals. Hydrogen in Metals I, Springer-Verlag, Berlin, West Germany, 1978, pp. 197–226.
[19] R.A. Oriani, Acta Metall. 18 (1970) 147–157.
[20] A.J. Kumnick, H.H. Johnson, Acta Metall. 28 (1980) 33–39.
[21] B.G. Pound, Acta Metall. Mater. 39 (1991) 2099–2105.
[22] S.M. Myers, M.I. Baskes, H.K. Birnbaum, J.W. Corbett, G.G. DeLeo, S.K. Estreicher, E.E. Haller, P. Jena, N.M. Johnson, R. Kirchheim, S.J. Pearton, M.J. Stavola, Rev. Mod. Phys. 64 (1992) 559–617.
[23] C. Bisong, H. Ichinose, M. Mori, Y. Ishida, Y. Bando, Phys. Rev. B 50 (1994) 5886–5889.
[24] H. Fukushima, H.K. Birnbaum, Acta Metall. 32 (1984) 851–859.

[25] B. Hohler, H. Kronmuller, Zeitschrift fur Physikalische Chemie Neue Folge 114 (1979) 93–108.
[26] C. Baker, H.K. Birnbaum, Acta Metall. 21 (1973) 865–872.
[27] D.H. Lassila, H.K. Birnbaum, Hydrogen Embrittlement of Nickel: Modeling of the Effect of Diffusive Segregation of Hydrogen on Intergranular Fracture, Metallurgical Society of AIME, Warrendale, PA, USA, 1986, pp. 259–271.
[28] D.H. Lassila, H.K. Birnbaum, Acta Metall. 35 (1987) 1815–1822.
[29] D.H. Lassila, H.K. Birnbaum, Acta Metall. 36 (1988) 2821–2825.
[30] J.-Y. Lee, J.-L. Lee, Philos. Mag. A 56 (1987) 293–309.
[31] D.H. Lassila, H.K. Birnbaum, Acta Metall. 34 (1986) 1237–1243.
[32] C.D. Beachem, Metall. Trans. A 3 (1972) 437–451.
[33] R. A. Oriani, Ber. Bunsenges. Phys. Chem. (West Germany) 76 (1972) 848–856.
[34] R.A. Oriani, P.H. Josephic, Scripta Metall. 6 (1972) 681–688.
[35] T. Tabata, H.K. Birnbaum, Scripta Metall. 17 (1983) 947–950.
[36] T. Tabata, H.K. Birnbaum, Scripta Metall. 18 (1984) 231–236.
[37] I.M. Robertson, H.K. Birnbaum, Acta Metall. 34 (1986) 353–366.
[38] G.M. Bond, I.M. Robertson, H.K. Birnbaum, Acta Metall. 35 (1987) 2289–2296.
[39] G.M. Bond, I.M. Robertson, H.K. Birnbaum, Acta Metall. 36 (1988) 2193–2197.
[40] D.S. Shih, I.M. Robertson, H.K. Birnbaum, Acta Metall. 36 (1988) 111–124.
[41] G.M. Bond, I.M. Robertson, H.K. Birnbaum, Acta Metall. 37 (1989) 1407–1413.
[42] P. Rozenak, I.M. Robertson, H.K. Birnbaum, Acta Metall. Mater. 38 (1990) 2031–2040.
[43] H.E. Hanninen, T.C. Lee, I.M. Robertson, H.K. Birnbaum, J. Mater. Eng. Perform. 2 (1993) 807–818.
[44] P.J. Ferreira, I.M. Robertson, H.K. Birnbaum, Mater. Sci. Forum 207–209 (1996) 93–96.
[45] P.J. Ferreira, I.M. Robertson, H.K. Birnbaum, Acta Mater. 46 (1998) 1749–1757.
[46] D.F. Teter, I.M. Robertson, H.K. Birnbaum, Acta Mater. 49 (2001) 4313–4323.
[47] J. Eastman, F. Heubaum, T. Matsumoto, H.K. Birnbaum, Acta Metall. 30 (1982) 1579–1586.
[48] T. Matsumoto, H.K. Birnbaum, Jpn. Inst. Metals 21 (1980) 493.
[49] P.J. Ferreira, I.M. Robertson, H.K. Birnbaum, Acta Mater. 47 (1999) 2991–2998.
[50] I. M. Robertson, H. K. Birnbaum (unpublished work).
[51] H.K. Birnbaum, Mechanisms of hydrogen induced failure of metals, in: Z.A. Foroulis (Ed.), Environmentally Sensitive Fracture of Metals, AIME, New York, 1979, pp. 326–360.
[52] R.A. Oriani, Corrosion 43 (1987) 390–397.
[53] M.S. Daw, M.I. Baskes, Phys. Rev. B 29 (1984) 6443–6453.
[54] C.L. Fu, G.S. Painter, J. Mater. Res. 6 (1991) 719–723.
[55] W.T. Geng, A.J. Freeman, R. Wu, C.B. Geller, J.E. Raynolds, Phys. Rev. B 60 (1999) 7149–7155.
[56] Y. Liang, P. Sofronis, Modell. Simul. Mater. Sci. Eng. 11 (2003) 523–551.
[57] Y. Liang, P. Sofronis, J. Eng. Mater. Technol., Trans. ASME 126 (2004) 368–377.
[58] Y. Liang, P. Sofronis, J. Mech. Phys. Solids 51 (2003) 1509–1531.
[59] J.P. Hirth, J.R. Rice, Metall. Trans. A 11A (1980) 1501–1511.
[60] S. Serebrinsky, E.A. Carter, M. Ortiz, J. Mech. Phys. Solids 52 (2004) 2403–2430.
[61] D.E. Jiang, E.A. Carter, Phys. Rev. B 70 (2004) 64101–64102.
[62] D.E. Jiang, E.A. Carter, Acta Mater. 52 (2004) 4801–4807.
[63] M. Dadfarnia, P. Sofronis, B.P. Somerday, J.B. Liu, D.D. Johnson, I.M. Roberston, Modeling issues on hydrogen-induced intergranular cracking under sustained load, in: B. P. Somerday, P. Sofronis (Eds.), Effects of Hydrogen on Materials, Jackson Lake Lodge, WI, 2009 in press.
[64] Y. Mishin, P. Sofronis, J.L. Bassani, Acta Mater. 50 (2002) 3609–3622.
[65] S. Asano, R. Otsuka, Scripta Metall. 10 (1976) 1015–1020.
[66] H. Hagi, S. Asano, R. Otsuka, J. Jpn. Inst. Metals 40 (1976) 796–801.
[67] N. Narita, C.J. Altstetter, H.K. Birnbaum, Metall. Trans. A (1982).
[68] L.S. Zevin, P. Rozenak, D. Eliezer, J. Appl. Crystallogr. 17 (1984) 18–21.
[69] M.E. Armacanqui, R.A. Oriani, Mater. Sci. Eng. 91 (1987) 143–152.
[70] N. Narita, H.K. Birnbaum, Scripta Metall. 14 (1980) 1355–1358.
[71] P. Rozenak, L. Zevin, D. Eliezer, J. Mater. Sci. 19 (1984) 567–573.

[72] A. Janko, S. Majchrzak, Acta Crystallographica 21 (1996) A81.
[73] A. Kimura, H.K. Birnbaum, Acta Metall. 35 (1987) 1077–1088.
[74] B.J. Makenas, H.K. Birnbaum, Acta Metall. 28 (1980) 979–988.
[75] G.R. Caskey Jr., Scripta Metall. 15 (1981) 1183–1186.
[76] B.A. Wilcox, G.C. Smith, Acta Metall. 12 (1964) 371–376.
[77] R.M. Latanision, R.W. Staehle, Scripta Metall. 2 (1968) 667–672.
[78] A.H. Windle, G.C. Smith, Metal Sci. J. 2 (1968) 187–191.
[79] A. H. Windle, G. C. Smith, Metal Sci. J. 4 (1970) 136–144.
[80] R.M. Latanision, H. Opperhauser Jr., Metall. Trans. A 5 (1974) 483–492.
[81] S. Asano, A. Kitamura, R. Otsuka, Scripta Metall. 12 (1978) 805–808.
[82] Y. Tobe, W.R. Tyson, Scripta Metall. 11 (1977) 849–852.
[83] A.M. Adair, Trans. Metall. Soc. AIME 236 (1966) 1613–1615.
[84] I.M. Bernstein, Scripta Metall. 8 (1974) 343–349.
[85] E. Lunarska, Z. Wokulski, Acta Metall. 30 (1982) 2173–2179.
[86] F. Zeides, Effect of Hydrogen on the Mechanical Properties and Fracture Properties of High Purity Aluminum. Ph.D. Thesis, University of Illinois, 1986.
[87] C.E. Buckley, H.K. Birnbaum, Physica B 241–243 (1997) 344–346.
[88] A. Kimura, H.K. Birnbaum, Scripta Metall. 21 (1987) 53–57.
[89] D. Eliezer, J. Mater. Sci. 19 (1984) 1540–1547.
[90] D.P. Abraham, C.J. Altstetter, Metall. Mater. Trans. A. 26A (1995) 2859–2871.
[91] D.G. Ulmer, C.J. Altstetter, Acta Metall. Mater. 39 (1991) 1237–1248.
[92] D.G. Ulmer, C.J. Altstetter, Acta Metall. Mater. 41 (1993) 2235–2241.
[93] R. Kirchheim, Acta Metall. 29 (1981) 835–843.
[94] R. Kirchheim, Acta Metall. 29 (1981) 845–853.
[95] J.A. Rodrigues, R. Kirchheim, Scripta Metall. 17 (1983) 159–164.
[96] C.W. Tien, C.J. Altstetter, Mater. Chem. Phys. 35 (1993) 58–63.
[97] G.B.A. Schuster, R.A. Yeske, C.J. Altstetter, Metall. Trans. A 11A (1980) 1657–1664.
[98] N.E. Paton, A.W. Thompson, Metall. Trans. A 13A (1982) 1531–1532.
[99] H. Matsui, A. Kimura, H. Kimura, The orientation dependence of the yield and flow stress of high purity iron single crystals doped with hydrogen, strength of metals and alloys, in: Proceedings of the 5th International Conference, vol. II, Pergamon, New York, NY, 1979, pp. 977–982.
[100] H. Matsui, H. Kimura, A. Kimura, Mater. Sci. Eng. 40 (1979) 227–234.
[101] S. Moriya, H. Matsui, H. Kimura, Mater. Sci. Eng. 40 (1979) 217–225.
[102] K. Oguri, S. Takaki, H. Kimura, Mater. Sci. Eng. 53 (1982) 223–232.
[103] A. Kimura, H. Matsui, H. Kimura, Mater. Sci. Eng. 58 (1983) 211–222.
[104] E. Pink, R.J. Arsenault, Prog. Mater. Sci. 24 (1979) 1–50.
[105] M. Wen, S. Fukuyama, K. Yokogawa, Acta Mater. 51 (2003) 1767–1773.
[106] J.S. Blakemore, Metall. Mater. Trans. A 1 (1970) 145–149.
[107] J.S. Blakemore, Metall. Mater. Trans. A 1 (1970) 151–156.
[108] A. Kimura, H.K. Birnbaum, Acta Metall. 38 (1990) 1343–1348.
[109] F.R.N. Nabarro, Theory of Crystal Dislocations, Oxford Press, Oxford, 1967.
[110] W.A. McInteer, A.W. Thompson, I.M. Bernstein, Acta Metall. 28 (1980) 887–894.
[111] I.M. Robertson, H.K. Birnbaum, Scripta Metall. 18 (1984) 269–274.
[112] M.V. Rodriguez, P.J. Ficalora, Scripta Metall. 20 (1986) 621–625.
[113] C. Hwang, I.M. Bernstein, Acta Metall. 34 (1986) 1011–1020.
[114] T.D. Le, I.M. Bernstein, Acta Metall. Mater. 39 (1991) 363–372.
[115] T.D. Lee, T. Goldenberg, J.P. Hirth, Hydrogen and plastic instability in deformed, spheroidized 1090 steel, in: Fourth International Conference on Fracture, vol. IIA, Pergamon, Oxford, UK, 1978, pp. 243–248.
[116] T.D. Lee, T. Goldenberg, J.P. Hirth, Metall. Trans. A 10A (1979) 439–448.
[117] O.A. Onyewuenyi, Scripta Metall. 18 (1984) 455–458.
[118] O.A. Onyewuenyi, J.P. Hirth, Metall. Trans. A 13A (1982) 2209–2218.

[119] C. San Marchi, B.P. Somerday, J. Zelinski, X. Tang, G.H. Schiroky, Metall. Mater. Trans. A 38 (2007) 2763–2775.
[120] D.F. Bahr, K.A. Nibur, B.P. Somerday, Acta Mater. 54 (2006) 2677–2684.
[121] F. Zeides, H. K. Birnbaum, Effect of Hydrogen on the Mechanical Properties and Fracture Behavior of High Purity Aluminum, Technical Report, ADA171214 (1986).
[122] J.K. Lin, R.A. Oriani, Acta Metall. 31 (1983) 1071–1077.
[123] T.C. Lee, D.K. Dewald, J.A. Eades, I.M. Robertson, H.K. Birnbaum, Rev. Sci. Instrum. 62 (1991) 1438–1444.
[124] D. Teter, P. Ferreira, I.M. Robertson, H.K. Birnbaum, An environmental cell TEM for studies of gas–solid interactions, in: New Techniques for Characterizing Corrosion and Stress Corrosion. TMS – Minerals, Metals & Materials Society, Warrendale, PA, 1996, pp. 53–71.
[125] G.M. Bond, I.M. Robertson, H.K. Birnbaum, Scripta Metall. 20 (1986) 653–658.
[126] T. Tabata, H.K. Birnbaum, Direct observation of the effect of hydrogen on dislocation behavior in iron, in: Dislocations in Solids, Yamada Science Foundation, 1985, pp. 219–222.
[127] D. Teter, The Effects of Hydrogen on the Deformation and Fracture Behavior of the Metastable Beta-Titanium Alloy Timetal 21S, Ph. D. Thesis, University of Illinois, 1996.
[128] W. Pesch, E. de Prieto, T. Schober, J. Less-Common Metals 84 (1982) 5–7.
[129] H. Saka, K. Noda, T. Imura, Cryst. Latt. Def. 4 (1973) 45–56.
[130] U.F. Kocks, A.S. Argon, M.F. Ashby, Thermodynamics and Kinetics of Slip, Pergamon Press, Oxford, 1975.
[131] E. Sirois, H.K. Birnbaum, Acta Metall. Mater. 40 (1992) 1377–1385.
[132] R.A. Oriani, P.H. Josephic, Acta Metall. 27 (1979) 997–1005.
[133] C. San Marchi, B.P. Somerday, X. Tang, G.H. Schiroky, Int. J. Hydrogen Energy 33 (2008) 889–904.
[134] K. Differt, U. Essmann, H. Mughrabi, Phys. Status Solidi A 104 (1987) 95–106.
[135] R.P. Tucker, M.S. Wechsler, S.M. Ohr, J. Appl. Phys. 40 (1969) 400–408.
[136] M. Victoria, N. Baluc, C. Bailat, Y. Dai, M.I. Luppo, R. Schaublin, B.N. Singh, J. Nucl. Mater. 276 (2000) 114–122.
[137] M.S. Wechsler, Dislocation channeling in irradiated and quenched metals, in: R.E. Reed-Hill (Ed.), The Inhomogeneity of Plastic Deformation, ASM, 1971, pp. 19–47.
[138] I.M. Robertson, J.S. Robach, H.J. Lee, B.D. Wirth, Acta Mater. 54 (2006) 1679–1690.
[139] A.E. Pontini, J.D. Hermida, Scripta Mater. 37 (1997) 1831–1837.
[140] J.P. Chateau, D. Delafosse, T. Magnin, Acta Mater. 50 (2002) 1507–1522.
[141] J.P. Chateau, D. Delafosse, T. Magnin, Acta Mater. 50 (2002) 1523–1538.
[142] D. Delafosse, G. Girardin, C. Bosch, J.P. Chateau, T. Magnin, Hydrogen–Dislocation Interactions in Nickel: Modelling and Experiments in Cyclic Plasticity, Minerals, Metals and Materials Society, Warrendale, PA, United States, 2003, pp. 191–200.
[143] G. Girardin, D. Delafosse, Scripta Mater. 51 (2004) 1177–1181.
[144] H.K. Birnbaum, Scripta Metall. Mater. 31 (1994) 149–153.
[145] P. Sofronis, Y. Liang, N. Aravas, Eur. J. Mech., A/Solids 20 (2001) 857–872.
[146] J.P. Hirth, J. Lothe, Theory of Dislocations, Wiley, New York, 1982.
[147] P. Sofronis, H.K. Birnbaum, J. Mech. Phys. Solids 43 (1995) 49–90.
[148] A.W. Cochardt, G. Schoek, H. Wiedersich, Acta Metall. 3 (1955) 533–537.
[149] F.C. Larche, J.W. Cahn, Interactions of Composition and Stress in Crystalline Solids, Compiled and Distributed by the NTIS, U.S. Department of Commerce, PB85179075, 1984 p. 34.
[150] J.P. Hirth, B. Carnahan, Acta Metall. 26 (1978) 1795–1803.